



ОБЪЕДИНЕННЫЙ ИНСТИТУТ ЯДЕРНЫХ ИССЛЕДОВАНИЙ JOINT INSTITUTE FOR NUCLEAR RESEARCH

4[67]-94

JINR RAPID COMMUNICATIONS

# Объединенный институт ядерных исследований Joint Institute for Nuclear Research

4[67]-94

# JINR RAPID COMMUNICATIONS

сборник



# ОГЛАВЛЕНИЕ CONTENTS

S.I.Fedotov, V.K.Lukyanov
Quasi-Classical Description of One-Nucleon Transfer Reactions
with Heavy Ions
С.И.Федотов, В.К.Лукьянов
Квазиклассическое описание однонуклонных передач
в реакциях с тяжелыми ионами
V.K.Lukyanov, A.V.Embulaev, V.P.Permyakov On Elastic and Inelastic Heavy Ion Scattering in the High-Energy Approximation В.К.Лукьянов, А.В.Ембулаев, В.П.Пермяков Упругое и неупругое рассеяние тяжелых ионов в высокоэнергетическом приближении
A.S.Fomichev, I.David, Yu.P.Kharitonov, S.M.Lukyanov, Yu.Ts.Oganessian, Yu.E.Penionzhkevich, V.P.Perelygin, N.K.Skobelev, O.B.Tarasov, R.Wolski
Experimental Study of Fission and Evaporation Cross Sections for <sup>6</sup> He + <sup>209</sup> Bi Reaction А.С.Фомичев, И.Давид, Ю.П.Харитонов, С.М.Лукьянов, Ю.Ц.Оганесян, Ю.Э.Пенионжкевич, В.П.Перелыгин, Н.К.Скобелев, О.Б.Тарасов, Р.Вольский
Экспериментальное изучение сечений деления
и испарения в реакции <sup>6</sup> He + <sup>209</sup> Bi
E.V.Chernykh, A.A.Nomofilov, V.V.Perelygin, V.I.Sharov, D.A.Smolin, V.N.Sotnikov, L.N.Strunov, S.A.Zaporozhets, A.V.Zarubin, V.E.Zhiltsov, L.S.Zolin, A.A.Izotov, T.Aono, T.Hasegawa, N.Horikawa, T.Iwata, A.Ogawa, T.Sasaki, S.Toyoda, T.Yamada, T.Dzikowski Tensor Analyzing Power T <sub>20</sub> for d <sup>↑</sup> + <sup>12</sup> C → p + X at Θ <sub>p</sub> = 0° in the Region of High Internal Momenta in the Deuteron Е.В.Черных, А.А.Номофилов, В.В.Перелыгин, В.И.Шаров, Д.А.Смолин, В.Н.Сотников, Л.Н.Струнов, С.А.Запорожец,
д.А.Смолин, В.Г.Сотников, Л.Г.Струнов, С.А.Запорожец, А.В.Зарубин, В.Е.Жильцов, Л.С.Золин, А.А.Изотов, Т.Аоно,
Т.Хасегава, Н.Хорикава, Т.Ивата, А.Огава, Т.Сасаки,
С.Тойода, Т.Ямада, Т.Дзиковски
Тензорная анализирующая способность Т
пля реакции $d^{\dagger} + {}^{12}C \rightarrow n + X$ при $\Theta = 0^{\circ}$
для реакции $d^{\dagger} + {}^{12}C \rightarrow p + X$ при $\Theta_p = 0^{\circ}$

A.S.Artiomov The Nuclotron Internal Targets A.C.Артемов Внутренние мишени в нуклотроне	40
I.A.Shelaev Actively Screened SC Magnets И.А.Шелаев Активно экранированные СП магниты	50
I.M.Sitnik, V.P.Ladygin, M.P.Rekalo Using of Polarized Target in Backward Elastic dp Scattering И.М.Ситник, В.П.Ладыгин, М.П.Рекало Использование поляризованной мишени в dp упругом рассеянии назад	56
E.V.Chernykh Application of Transputers in the Data Acquisition System of the INESS-ALPHA Spectrometer E.В.Черных Применение транспьютеров в системе сбора данных спектрометра ИНЕСС-АЛЬФА	62
Yu.A.Troyan, V.N.Pechenov, E.B.Plekhanov, S.G.Arakelian, A.Yu.Troyan, V.I.Moroz, A.P.Ierusalimov, A.P.Stelmakh Narrow Dibaryon Resonances with Isotopic Spin I = 2 Ю.А.Троян, В.Н.Печенов, Е.Б.Плеханов, С.Г.Аракелян, А.Ю.Троян, В.И.Мороз А.П.Иерусалимов, А.П.Стельмах Узкие дибарионные резонансы	
с изотопическим спином I = 2	67

es not be a compared to

# QUASI-CLASSICAL DESCRIPTION OF ONE-NUCLEON TRANSFER REACTIONS WITH HEAVY IONS

# S.I.Fedotov, V.K.Lukyanov

The heavy-ion one-nucleon transfer reactions are considered using the distorted waves obtained in the framework of the high energy approximation (HEA) method in the three-dimensional quasi-classics. The bound state nucleon wave function is presented in a form of the derivative of the Fermi function. The cross section is obtained in the analytic form, showing the main physical features of the reaction mechanism. The results of calculations are in good agreement with experimental data.

The investigation has been performed at the Bogoliubov Laboratory of Theoretical Physics, JINR.

### Квазиклассическое описание однонуклонных передач в реакциях с тяжелыми ионами

### С.И.Федотов, В.К.Лукьянов

Рассматриваются однонуклонные передачи в реакциях с тяжелыми ионами с использованием искаженных волн, полученных в рамках метода высокоэнергетического приближения (ВЭП) в трехмерной квазиклассике. Волновая функция связанного состояния нуклона выбирается в виде производной от ферми-функции. Дифференциальные сечения получаются в аналитическом виде, что позволяет понять основные свойства механизма реакций. Результаты расчетов находятся в хорошем согласии с экспериментальными данными.

Работа выполнена в Лаборатории теоретической физики им. Н. Н. Боголюбова ОИЯИ.

#### 1. Introduction

The traditional consideration of the high-energy transfer reactions with heavy ions is based on a partial wave representation of the *in*- and *out*-distorted waves. To this aim, at energies of several dozen MeV per nucleon, it is necessary to numerically calculate a lot of partial waves which introduce both the hard numerical problems and difficulties in searching for the physics of the reaction mechanism. To avoid these difficulties, we apply the HEA-method developed for calculations of the three-dimensional quasi-classical wave functions and for the corresponding matrix elements with these

functions included [1,2]. The method can be applied under the conditions kR >> 1, E >> V and  $\theta > \theta_c \cong |V|/E$ , where  $\theta_c$  is the classical deflection angle. This latter is introduced to include distortion of the straigt-line trajectories of motion, the important point in investigating the heavy-ion collisions. On the whole, this gives us the possibility of avoiding complicated numerical calculations and obtaining, in the framework of the DWBA, analytical expressions for qualitative physical estimations and for a quantitative comparison with experimental data.

#### 2. Differential Cross Section

For simplicity, we consider the reaction  $a + A \rightarrow b + B$  with transfer of a spinless x-particle when the corresponding cross section and the amplitude in the zero-range approximation are as follows:

$$\frac{d\sigma}{d\Omega} = \frac{m_{\alpha}m_{\beta}}{(2\pi h^2)^2} \frac{k_{\beta}}{k_{\alpha}} \frac{2J_B + 1}{(2J_A + 1)(2J_a + 1)} \sum_{l} \frac{S_l}{2l + 1} \left| \tilde{T}_l^{tr} \right|^2, \quad (2.1)$$

$$\tilde{T}_{l}^{tr} = -D_{0} \int d\mathbf{r} \, \Psi_{\beta}^{(-)*}(\mathbf{r}) \, \Psi_{\alpha}^{(+)}(\mathbf{r}) \, \Re_{l}(\mathbf{r}) \, Y_{l0}^{*}(\hat{\mathbf{r}}), \tag{2.2}$$

where

$$D_0 = 8\pi \sqrt{(m_a h^2/2m_x m_b)^3 \varepsilon_{xb}}$$

depends on the structure of an incident particle,  $\varepsilon_{xb}$  is the separation energy and  $\Re_{\ell}(r)$  is the radial wave function of the x-particle in the final nucleus B. The latter has the asymptotic behaviour  $\exp(-k_{\ell}r)/r$  and goes to the constant as  $r \to 0$ . We have emphasized that the main effect in heavy ion reactions comes from the region near the interaction radius. This means that the behaviour of the function  $\Re_{\ell}$  at r << R is of no importance, and one can select it in the form

$$\Re_{l}(r) = \frac{\sqrt{6a_{l}}}{r} \frac{df_{s}(r, R, a_{l})}{dr}, \qquad (2.3)$$

where

$$f_s = \frac{\sinh \frac{R}{a_l}}{\cosh \frac{R}{a_l} + \cosh \frac{r}{a_l}} \cong \frac{1}{1 + \exp \frac{r - R}{a_l}}$$
 (2.4)

is the symmetrized Fermi function having the asymptotics  $\exp(-k_l r)/r$  and being a constant at r=0; the function (2.3) is normalized to 1, and the «diffuseness» of the transition region is to be taken  $a_l=1/k_l$ , where  $k_l=1/k_l$ 

= 
$$\sqrt{2m_{\chi}\varepsilon_{l}/h^{2}}$$
 with  $\varepsilon_{l}$ , the separation energy.

Inserting (2.3) into (2.2), we get the amplitude of the typical form inherent in HEA. Moreover, here we can use the quasi-elastic approximation because the loss of energy in the reaction is comparatively small and  $E_{\alpha} \cong E_{\beta}$ . Thus, the QC-distorted waves are calculated as in the elastic channel. The product  $\Psi_{\beta}^{(-)*}\Psi_{\alpha}^{(+)}$  has the following form [1,2]

$$\Psi_{\beta}^{(-)*}\Psi_{\alpha}^{(+)} = \exp(i\,\widetilde{\Phi}),\tag{2.5}$$

where

$$\widetilde{\Phi} = 2\overline{a}_0 + \widetilde{\beta}\mu + n_1\mu^2 + c_1\mu^3 + + n_2(1 - \mu^2)\cos^2\overline{\varphi} + c_2\mu (1 - \mu^2)\cos^2\overline{\varphi}$$
 (2.6)

and  $\widetilde{\beta}$ , c and n are expressed through r, parameters of the potentials,  $\alpha = \sin{(\theta/2)}$ , and  $\alpha_c \cong \frac{1}{2E} [V(R_t) + V_C(R_t) + iW(R_t)]$ , taken at the radius  $R_t$  of the external limited trajectory of motion. For example,

$$\widetilde{\beta} = \widetilde{q}r = q_{ef}r + 2k_{\delta}\alpha r; \qquad q_{ef} = 2k(\alpha - \alpha_{c});$$

$$k_{\delta} = -\left[B^{V} + iB^{W} + B^{C}\left(3 - \frac{r^{2}}{R_{C}^{2}}\right)\right], \qquad (2.7)$$

where

$$B^V = \frac{V_0}{hv};$$
  $B^W = \frac{W_0}{hv};$   $B^C = \frac{Z_1 Z_2 e^2}{R_C hv}.$ 

The other functions in (2.6) are done in [1].

We can see that now the integrand (2.2) contains in the exponent a typical power dependence on the variables r and  $\mu$ . Keeping in mind that  $dr = -r^2 dr d\mu d\bar{\varphi}$ , we first integrate in (2.2) over  $d\mu$  by parts

$$I_{l} = \int_{-1}^{+1} d\mu \exp(i\widetilde{\Phi}) Y_{l0} \cong$$

$$\cong -i \left( \frac{\exp(i\widetilde{\Phi})}{\partial \widetilde{\Phi}/\partial \mu} \Big|_{+1} - (-)^{l} \frac{\exp(i\widetilde{\Phi})}{\partial \widetilde{\Phi}/\partial \mu} \Big|_{+1} \right) Y_{l0}(1), \tag{2.8}$$

neglecting the second term having the smallness  $(kR)^{-2}$ . The result is

$$I_{l} = -i\sqrt{\frac{2l+1}{4\pi}} \exp(2i\overline{a}_{0} + in_{1}) [I^{(+)} - (-)^{l}I(-)];$$

$$I^{(\pm)} = \frac{\exp[\pm i(\widetilde{\beta} + c_{1})]}{\Delta_{(\pm)} \mp \delta_{(\pm)} \cos^{2}\overline{\varphi}};$$
(2.9)

$$\Delta_{(\pm)} = \tilde{\beta} + 3c_1 \pm 2n_1;$$
  $\delta_{(\pm)} = 2(n_2 \pm c_2).$  (2.10)

Then, the integration over  $d\overline{\varphi}$  can be performed with the help of a table integral. Thus, we can write the amplitude (2.2) in the form of a one-dimensional integral [1,2]:

$$\widetilde{T}_{l}^{tr} = -iD_{0}\sqrt{6\pi a_{l}(2l+1)} e^{i2\overline{a}_{0}} \int_{0}^{\infty} \frac{df_{s}}{dr} \{F^{(+)}(r) - (-)^{l}F^{(-)}(r)\} dr, (2.11)$$

where

$$F^{(\pm)}(r) = \frac{\exp[\pm i\phi^{\pm}]}{L^{\pm}} = \exp[\pm i\Phi^{\pm}];$$
 (2.12)

$$\Phi^{\pm} = \phi^{\pm} - \ln L^{\pm}; \qquad \phi^{\pm} = f_1 r \pm f_2 r^2 + f_3 r^3;$$

$$L^{\pm} = \sqrt{(f_1 + f_4 r + f_5 r^2)(f_1 \pm f_6 r + f_7 r^2)}$$
(2.13)

with f, the functions of parameters of the potentials,  $\alpha$  and  $\alpha$ :

$$\begin{split} f_1 &= 2k \left(\alpha - \alpha_c\right) - 2(B^V + iB^W + 3B^C\right) \alpha; \qquad f_2 &= \left(\frac{B^V}{R_V} + i\frac{B^W}{R_W}\right) (1 - \alpha^2); \\ f_3 &= \frac{2B^C}{R_C^2} \left(1 - \frac{2}{3}\alpha^2\right) \alpha; \qquad f_4 &= 2\left(\frac{B^V}{R_V} + i\frac{B^W}{R_W}\right) \alpha^2; \\ f_5 &= \frac{2B^C}{R_C^2} \left(1 - 2\alpha^2\right) \alpha; \qquad f_6 &= 2\left(\frac{B^V}{R_V} + i\frac{B^W}{R_W}\right) (1 - 2\alpha^2); \\ f_7 &= \frac{2B^C}{R_C^2} (5 - 6\alpha^2) \alpha. \end{split} \tag{2.14}$$

Integrals of the type (2.11) can be calculated in the analytical form if one uses the second order poles on the complex r-plane of the derivative

 $df_s/dr$  in the region of the nuclear surface at  $r_n^{\pm} = R \pm i\pi (2n + 1) a_l$ , where n = 0, 1, 2... It is easy to show that the main contribution to (2.11) is coming from the two poles closest to the real axes of r. Then, the final expression for the differential cross section is as follows:

$$\frac{d\sigma}{d\Omega} = 6\pi a_l^3 S_l D_0^2 \frac{2J_B + 1}{(2J_A + 1)(2J_A + 1)} e^{4B^W R_W} \left| \left[ \frac{d}{dr} \exp(i\Phi^{(+)}) \right]_{r_0^+} + \right. \\
\left. + (-)^l \left[ \frac{d}{dr} \exp(-i\Phi^{(-)}) \right]_{r_0^-} \right|^2.$$
(2.15)

Thus, we can conclude that here we have the general exponential decrease at angles  $\theta > \theta_c$ , depending on the acting thickness  $a_l$  in the region of the surface of transition [3]. The magnitude of the cross section is determined by the slope of a «tail» of a bound state function in the final nucleus B.

#### 3. Conclusion

Figure 1 shows calculations (solid line) and comparisons with experimental data (squares) from [4]. We can see that the differential cross section is decreasing with the angle of scattering as an exponential function with a slope determined by the thickness parameter  $a_l$  characterizing the corresponding form factor behaviour in the surface area of interaction. In Fig.1, the solid line corresponds to  $a_l = 0.4$  fm. The spectroscopic factor was taken to equal 1. The other parameters are  $V_0 = 50$  MeV,  $W_0 = 19$  MeV,  $r_{0v} = r_{0w} = r_{0c} = r_{0t} = 1.2$  fm.

In our calculations the absolute values of theoretical cross sections are presented. The absolute values of the cross sections and their form strongly depend on the imaginary part of the complex potential. In the case of a potential when  $W_0$  is very small, the main part of differential cross section  $-\exp(-2\pi a_l k(\Theta-\Theta_c))\cos^2(kR\Theta)$  for even l (solid line in Fig.2) and  $-\exp(-2\pi a_l k(\Theta-\Theta_c))\sin^2(kR\Theta)$  for odd l (dashed line in Fig.2). We see that the cross section is decreasing with the angle of scattering as an

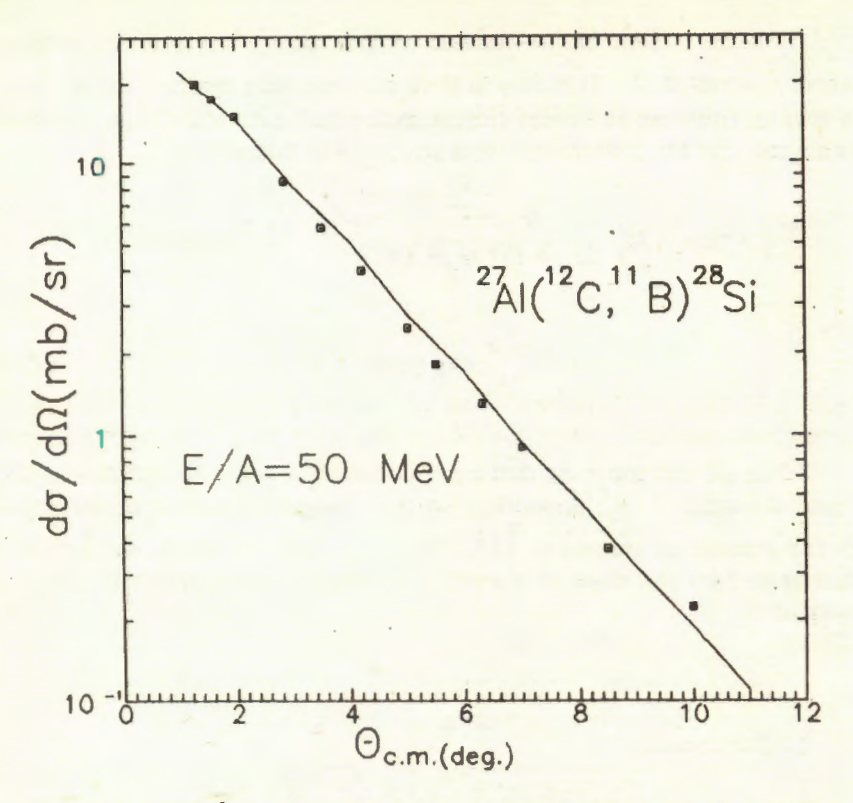


Fig. 1. The transfer reaction cross sections:  ${}^{12}C + {}^{27}AI \rightarrow {}^{11}B + {}^{28}Si; E = 50 \text{ MeV/n},$  exp. data (squares) from [4], solid lines — theory

exponential function and simultaneously oscillates. The oscillation with even l are out phase with those with odd l. The solid line with stars corresponds to  $W_0 = 10$  MeV, when the oscillations start to appear.

We can summarize that investigations of heavy ion collisions in the quantum region of scattering angles  $\Theta > \Theta_c$ , outside the limited trajectories of motion, are very sensitive to the precise structure of a nuclear-nuclear interaction. For instance, the slope of the curves with  $\Theta$  feels the «thickness» of the acting region in the corresponding channel. It may be used also for searching the «halo» distributions of nuclei in the radioactive beams which now become available. We hope that the HEA-method suggested can be successfully used in both the qualitative and quantitative analysis of direct reactions.

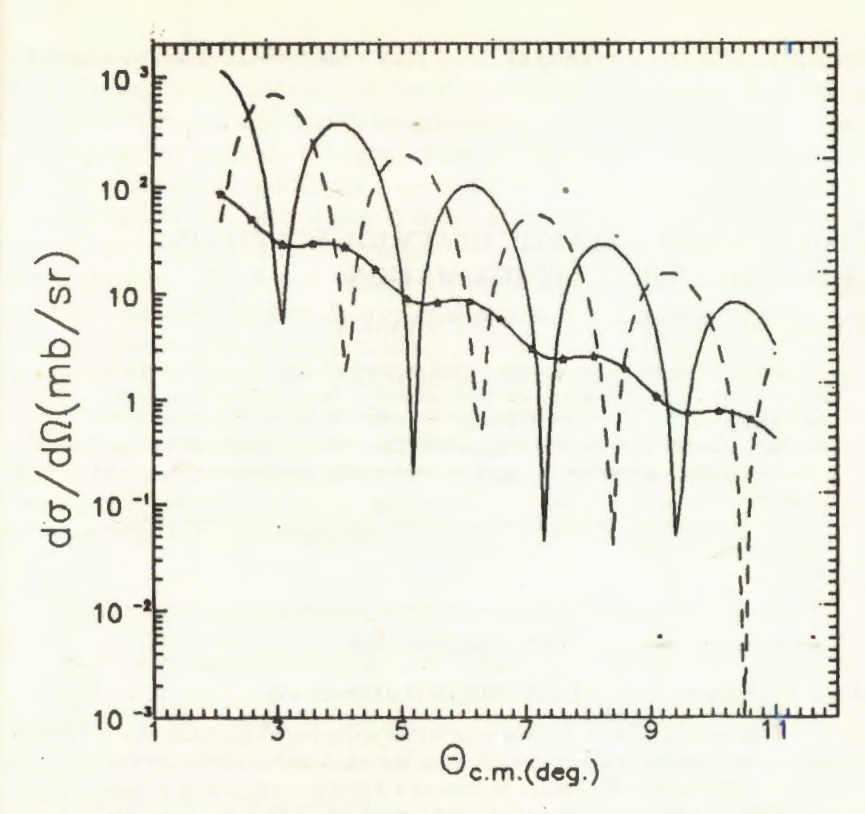


Fig. 2. The solid line shows the cross section calculated for the same reaction by using  $W_0=1~{\rm MeV}$ , l=2, the dashed line shows the cross section calculated by using  $W_0=1~{\rm MeV}$ , l=1 and the solid line with stars shows the cross section calculated by using  $W_0=10~{\rm MeV}$ , l=2

## References

- 1. Lukyanov V.K. JINR Preprint E4-93-314, Dubna, 1994.
- Lukyanov V.K. Proc. Int. School-Seminar on HI Phys., JINR E7-93-274, Dubna, 1993, v.2, p.129.
- Lukyanov V.K., Gridnev K.A., Embulaev A.V. Bull. of Russ. Acad. of Sc., Physics, 1994, v.58, p.19 (in Russian Izv. RAN, ser. fiz., 1994, v.58, p.23).
- 4. Winfield J.S. et al. Phys. Rev., 1989, v.C39, p.1395.

# ON ELASTIC AND INELASTIC HEAVY ION SCATTERING IN THE HIGH-ENERGY APPROXIMATION

V.K.Lukyanov, A.V.Embulaev\*, V.P.Permyakov

Using the high-energy approximation method for the three-dimensional quasi-classics, elastic and inelastic cross sections of heavy ions at large angles are calculated. The role of the deflection angle introduced in the theory and of the parameters of an interaction is discussed. The corresponding amplitudes are obtained in analytic forms and a good agreement with experimental data is also obtained.

The investigation has been performed at the Bogoliubov Laboratory of Theoretical Physics, JINR.

Упругое и неупругое рассеяние тяжелых ионов в высокоэнергетическом приближении

В.К.Лукьянов, А.В.Ембулаев, В.П.Пермяков

Дифференциальные сечения упругого и неупругого рассеяния тяжелых ионов на ядрах рассчитаны на основе высокоэнергетического приближения для квазиклассического рассеяния в поле комплексного потенциала. Проанализирована роль отклонения траектории от прямой линии. Амплитуды рассеяния получены в аналитическом виде. Достигнуто хорошее согласие результатов расчета с экспериментальными данными.

Работа выполнена в Лаборатории теоретической физики им.Н.Н.Боголюбова ОИЯИ.

#### 1. Introduction

Elastic and inelastic scattering of alpha-particles, light and heavy ions on nuclei at energies E >> V is very sensitive to the parameters of an interaction potential and also to the detailed behavior of the structure characteristic such as the density distributions, transition matrix elements and so on. Indeed, in this case the corresponding wave length  $\lambda$  is much smaller than typical dimensions of a nucleus, the radius R and thickness a of a boundary of the nuclear interaction. Moreover, a specific problem appears at large scattering angles when the cross section is as a rule exponentially decreasing because the sets of partial wave decompositions become the sign-

<sup>\*</sup>Saratov State University, Saratov, Russia

alternative ones and, therefore, one needs to keep in the computer memory a lot of partial phases. One of the ways to decrease these difficulties is to use one-dimensional quasi-classics for calculating the partial phases and then to develop special methods of summing up the corresponding partial sets [1]. However, the initial conditions  $E \gg V$ ,  $kR \gg 1$  may be used themselves for developing the approach where it is not necessary to use the partial wave expansion for the elastic and inelastic scattering amplitude. In particular, the method was developed based on three-dimensional quasi-classics that operates not with the one-dimensional partial waves but directly with the theree-dimensional action function [2-4]. A deflection of the classical trajectory of motion on the straight line is included which plays an important role especially in the case of the heavy-ion scattering. We have used the realistic complex nuclear and Coulomb potentials and made comparison with experimental data obtained for the heavy-ion beams at energies about one hundred MeV per nucleon. Below we apply this method to the processes of elastic and inelastic scattering

# 2. Elastic Scattering

Heavy ion elastic scattering at energies larger than several dozen MeV per nucleon is just the process to which the method mentioned above can be adjusted. To this aim we use the elastic scattering amplitude obtained in [3] for large angles  $\theta > (1/kR)$  and  $\theta > \theta_c \cong (|V|/E)$  covering in practice a wide region of scattering angles

$$T^{el} = -\frac{m}{2\pi h^2} \int d\mathbf{r} \Psi_{\mathbf{k}_f}^{(-)*} V \Psi_{\mathbf{k}_l}^{(+)} =$$

$$= -\frac{m}{2\pi h^2} \int d\mathbf{r} (V_N + V_C) \exp\{i \, \mathbf{q}_{ef} \, \mathbf{r} + i \, \Phi(\mathbf{r})\}, \qquad (2.1)$$

where [2]

$$\Phi = \Phi_i^{(+)} + \Phi_f^{(-)};$$

$$\Phi^{(\pm)} = -\frac{1}{h\nu} \int_{\overline{+}z}^{\infty} \left[ V_N(\sqrt{\rho^2 + \lambda^2}) + V_C(\sqrt{\rho^2 + \lambda^2}) \right] d\lambda, \qquad (2.2)$$

and the potentials

$$V_N = V + iW = V_0 f_V(r) + iW_0 f_W(r),$$
 (2.3)

$$V_{C} = \frac{Z_{1}Z_{2}e^{2}}{R_{C}} \int \frac{\rho_{c}(x)dx}{|r - x|}, \ \rho_{c} = \rho_{0}f_{c}(r)$$
 (2.4)

with the charge density distribution  $\rho_c(r)$  and the effective momentum transfer  $\mathbf{q}_{ef} = \mathbf{q} - \mathbf{q}_c$ , where  $\mathbf{q} \, \mathbf{l} \, \mathbf{q}_c$ ,  $q_{ef} = 2k(\alpha - \alpha_c)$ ,  $\alpha = \sin(\theta/2)$ , and  $\alpha_c \cong \frac{1}{2E} \left[ V(R_t) + V_c(R_t) + iW(R_t) \right]$ , taken at the radius  $R_t$  of the external limited trajectory of motion. All the distribution functions are taken in the form of the Fermi-function

$$f_p(r) = \frac{1}{1 + \exp{\frac{r - R_p}{a_p}}}.$$
 (2.5)

Thus, the scattering amplitude consists of three terms:

$$T^{el} = T_V^{el} + iT_W^{el} + T_C^{el}. (2.6)$$

Substituting (2.4) into  $T_C^{el}$  we obtain the 6-dimensional integral. It can be transformed to the 3-dimensional one if one expands the phase  $\Phi$  in u = r - x and then integrates over du [5]

$$T_C^{el} = -\frac{m}{2\pi\hbar^2} \int d \, r \nu_c(r) \, \exp \left\{ i \, \widetilde{\Phi}(r) \right\}, \, \nu_c(r) = \frac{Z_1 Z_2 e^2 \rho_0}{q_e^2 R_C} f_c(r),$$

$$\widetilde{\Phi}(\mathbf{r}) = \mathbf{q}_{ef}\mathbf{r} + \Phi(\mathbf{r}), \tag{2.7}$$

where  $q_e \cong q_{ef}$  and  $v_c(r)$  plays the role of a quasi-potential of scattering on a spread nuclear charge. Now each of the terms of the scattering amplitude (2.6) has the same form:

$$T_p^{el} = -\frac{m}{2\pi h^2} \int d \, r Y_p f_p(r) \exp \{i \, \widetilde{\Phi}(r)\},$$
 (2.8)

where  $Y_p$  is the «strength» of the corresponding part of the whole potential.

It has been shown in [2,4] that in calculating the whole quasi-classical phase  $\widetilde{\Phi}$  one may limit oneself to the step nuclear potential and the inside-of-R part of a Coulomb potential. In this case the phase has a rather simple form with a typical power dependence on the variables of integration r,  $\mu = \cos \overline{\theta}$  and  $\cos \overline{\phi}$ . It is written as follows:

$$\widetilde{\Phi} = 2\overline{a}_0 + \widetilde{\beta}\mu + n_1\mu^2 + c_1\mu^3 +$$

$$+ n_2(1-\mu^2)\cos^2\overline{\varphi} + c_2\mu(1-\mu^2)\cos^2\overline{\varphi}, \qquad (2.9)$$

where  $\tilde{\beta}$ , c and n are expressed through  $a_n$ . For example,

$$\widetilde{\beta} = 2k(\alpha - \alpha_c)r + \overline{\beta};$$

$$\overline{\beta} = -\frac{2}{h\nu} \left[ (V_0 + iW_0) + \frac{Z_1 Z_2 e^2}{2R_C} (3 - \frac{r^2}{R_C^2}) \right] \alpha r. \tag{2.10}$$

Now, keeping in mind that  $dr = -r^2 dr d \mu d \overline{\varphi}$ , one can integrate in (2.8) over  $d\mu$  by parts

$$I = \int_{-1}^{+1} d\mu \exp \left[i\widetilde{\Phi}\left(r,\mu,\widetilde{\phi}\right)\right] = -i \frac{\exp\left(i\widetilde{\Phi}\right)}{\partial\widetilde{\Phi}/\partial\mu} \Big|_{-1}^{+1} +$$

+ 
$$i \int d\mu \exp(i\widetilde{\Phi}) \frac{\partial^2 \widetilde{\Phi}/\partial \mu^2}{(\partial \widetilde{\Phi}/\partial \mu)^2}$$
, (2.11)

neglecting the second term, having the smallness  $(kR)^{-2}$ . The result is

$$I = -i \exp(2i\overline{a}_0 + in_1)[I^{(+)} - I^{(-)}];$$

$$I^{(\pm)} = \frac{\exp\left[\pm i(\widetilde{\beta} + c_1)\right]}{\Delta_{(\pm)} \mp \delta_{(\pm)} \cos^2 \overline{\varphi}}; \qquad (2.12)$$

$$\Delta_{(\pm)} = \tilde{\beta} + 3c_1 \pm 2n_1; \quad \delta_{(\pm)} = 2(n_2 \pm c_2). \tag{2.13}$$

Then the integration over  $d\overline{\varphi}$  is performed with the help of a table integral. Thus, we can write the amlitude (2.8) in the form of a one-dimensional integral [2]:

$$T_p^{el} = \frac{im}{\hbar^2} Y_p \int_0^\infty f_p(r) \Big\{ F_p^{(+)}(r) - F_p^{(-)}(r) \Big\} dr, \qquad (2.14)$$

where

$$F_p^{(\pm)}(r) = \frac{r \exp[\pm i(\widetilde{q}r + c_1)] \exp[i(2\overline{a}_0 + n_1)]}{\widetilde{q}L(\pm)};$$

$$L(\pm) = \frac{1}{\overline{\beta}} \sqrt{\Delta_{(\pm)}(\Delta_{(\pm)} - \delta_{(\pm)})}. \tag{2.15}$$

Integration in (2.14) can be done [2,4] if one uses the properties of the Fermi-function, which has poles  $r_n^{(\pm)} = R \pm i\pi a(2n+1)$ , (n=0,1,2...) on the complex r-plane. In practice, for the typical nuclear parameters it is enough to take into account only a couple of poles  $r_0^{(\pm)} = R \pm ix_0$  nearest to the real axis («two-pole approximation»), because every next pair contributes approximately an order smaller than the previous one. Then, we have

$$T_p^{el} = -\frac{im}{h^2} Y_p 2\pi i a [F^{(+)}(r_0^{(+)}) + F^{(-)}(r_0^{(-)})].$$
 (2.16)

Substituting into (2.16) the corresponding poles one can easily find that the amplitude, roughly speaking, behaves as an exponential function, depending on the exponent  $-2\pi ak \sin \theta/2$  and oscillating with a frequency as a function of the radius R.

# 3. Inelastic Scattering

For calculating the inelastic scattering of light and heavy ions with excitation of the collective nuclear states we have used DWBA with the relative-motion QC-wave functions whose phases are calculated as it is shown in Sec.2. The energy change in the out-channel is neglected since usually  $E_{ex} \ll E$ . The transition interaction is constructed as usual with the help of derivatives in small quadrupole and octupole additions  $\delta R = R \sum_{i=1}^{\infty} \alpha_{LM} Y_{LM}^*(\hat{r})$  to the radius of a potential in the elastic channel. The result for the amplitude is the same as if one uses the sudden approximation

$$T^{in} = (J_f M_f | \hat{T}_V^{el} + i \hat{T}_W^{el} + \hat{T}_C^{el} | J_i M_l), \tag{3.1}$$

where

$$\hat{T}_{p}^{el} = -\frac{m}{2\pi h^{2}} \int d\mathbf{r} Y_{p} f_{p}(r, R + \delta R) \Psi^{(-)*} \Psi^{(+)}$$
 (3.2)

is the operator, depending on the internal nuclear coordinates  $\alpha_{LM}$ . Then, substituting (3.2) into (3.1) we get

$$T_p^{in} = \sum_{IM} (J_f M_f | \alpha_{LM} | J_i M_i) \widetilde{T}_{(p)LM}^{in},$$
 (3.3)

where

$$\tilde{T}_{(p)LM}^{in} = -\frac{m}{2\pi h^2} Y_p R \int d\mathbf{r} \ \Psi^{(-)*} \Psi^{(+)} d \frac{f_p}{dR} Y_{LM}^*. \tag{3.4}$$

Transforming the structure matrix element in (3.3) through the reduced one and using the definition of  $B\downarrow(EL)$ -transition, one can write the inelastic cross section:

$$\frac{d\sigma}{d\Omega} = \frac{(2J_f + 1)}{(2J_i + 1)} \frac{1}{(2L + 1)} \sum_{LM} \frac{B \downarrow (EL)}{D_I^2} |\tilde{T}_{LM}^{in}|^2$$
 (3.5)

with

$$D_L = Z_2 e \rho_0 R_C J_L^c; \quad J_L^c = \int \frac{df_c}{dR_C} r^{L+2} dr \cong R_C^{L+2}.$$
 (3.6)

One can show that all the terms with  $M \neq 0$  may be neglected because of the additional fast oscillations in integrands as compared with the term M=0. Then, the principal difference of the inelastic amplitude from the elastic one appears in integral over  $d\mu$ , because now in the upper and lower limits  $\mu=\pm 1$  we have to take into account the relation

$$Y_{L0}(-\mu) = (-1)^L Y_{L0}(+\mu),$$
 (3.7)

which changes the sign of the second term in the inelastic analog of eq. (2.14) for odd L. Indeed, using the relation  $df_p/dR = -df_p/dr$ , we get:

$$\widetilde{T}_{p}^{in} = -\frac{im}{h^{2}} Y_{p} Y_{L0}(1) R \int_{0}^{\infty} dr \frac{df_{p}}{dr} \left\{ F_{p}^{(+)}(r) - (-1)^{L} F_{p}^{(-)}(r) \right\}. \quad (3.8)$$

This integral can be calculated in an analytical form if one uses the second order poles on the complex plane of the derivative df/dr. However, we show another way. Indeed, bearing in mind that the  $F^{(\pm)}$ -functions rapidly

oscillate with increasing r because of the exponent  $\tilde{q}r >> 1$ , one can integrate in (3.8) by parts

$$\int_{0}^{\infty} \frac{df_{p}}{dr} F_{p}^{(\pm)} dr = -\int_{0}^{\infty} f_{p} \frac{dF_{p}^{(\pm)}}{dr} dr - O\left(\frac{1}{(\tilde{q}r)^{2}}\right). \tag{3.9}$$

So, substituting (3.9) into (3.8) we get a form like (2.14) for elastic scattering with some additions in the integrand, namely, the factor  $\tilde{q}R$  and the multiplier  $(-1)^L$  before the second term:

$$\widetilde{T}_{p}^{in} = \frac{im}{h^{2}} Y_{p} Y_{L0}(1) R \widetilde{q} \int_{0}^{\infty} dr f_{p}(r) \left( F_{p}^{(+)}(r) - (-)^{L} F_{p}^{(-)}(r) \right). \quad (3.10)$$

Subsequent calculations are the same as in the case of elastic scattering, using the two-pole approximation.

#### 4. Conclusion

Calculations of differential cross sections for elastic and inelastic scattering within the two-pole approximation are presented in Figs.1 and 2 in comparison with the experimental data from [6]. One can see a rather good agreement in the range of scattering angles  $\theta > \theta_c \cong 2^\circ$  in coincidence with the initial assumptions of the HEA-method. For each set of colliding nuclei we got the same interaction parameters for elastic and inelastic channels excluding the absorption  $W_0$  that occurred to be about 10% as small as that in the elastic channel. The depths of potential wells are in

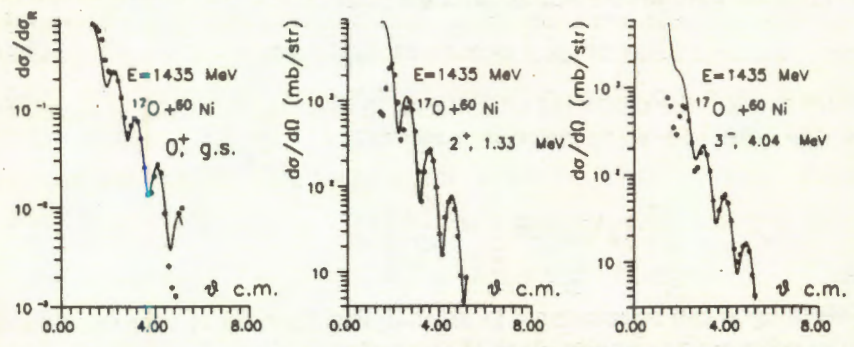


Fig.1. The heavy ion elastic and inelastic cross sections  $^{17}O+^{60}Ni$ ;  $E_{lab}=1435$  MeV; exp. data from [6]; solid lines — theory

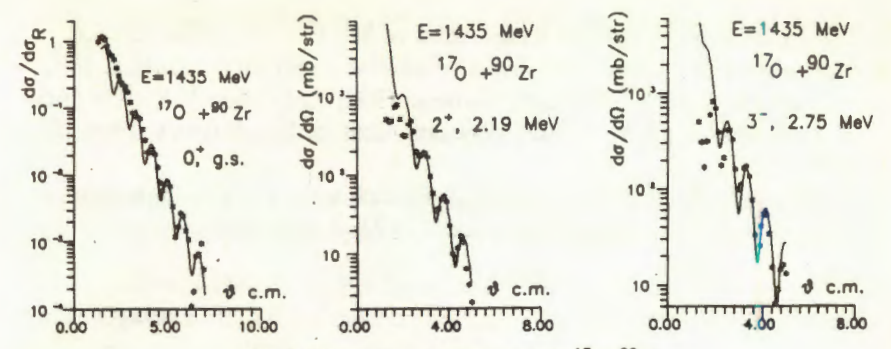


Fig. 2. The same as in Fig. 1, but for <sup>17</sup>O+<sup>90</sup>Zr

limits of  $V_0 = 60-70$  MeV and  $W_0 = 5-6$  MeV, the B(EL)-transitions obtained are approximately twice those cited in [6]. The most interesting result is that the thickness parameters for inelastic channels are about twothree times as small as those for elastic channels, where we have  $a_{el} = 0.55 - 0.6$  fm. This might signify that in collective excitations of nuclei not all the particle states take part in forming the transition matrix elements. Otherwise, in elastic scattering the «tail» of a potential is formed from the whole set of one-particle states. It is easy to see from (3.10) that the oscillating part of the amplitude as a function of the scattering angle is the cos- or sin-function depending an L-even or odd, respectively. In this case the cross section will have visible oscillations which coincide for excitations of the even collective states in their phases with the elastic scattering oscillations. We can summarize that investigations of heavy ion collisions in the quantum region of scattering angles  $\theta > \theta_c$ , outside the limited trajectories of motion, are very sensitive to the precise structure of a nuclearnuclear interaction. For instance, the slope of curves with  $\theta$  feels the «thickness» of the acting region in the corresponding channel. This may be used also in searching for the «halo» distributions of nuclei in the radioactive beams which now become available. We hope that the HEA-method suggested can be successfully used in both the qualitative and quantitative analyses of scattering processes and direct reactions.

The authors are grateful to Dr.R.Roussel-Chomaz for providing the tables on elastic and inelastic scattering data.

#### Reference

- Ford K.W., Wheeler J.A. Ann. Phys., 1959, 7, p.259; Zagrebaev V.I. Ann. Phys., 1990, 197, p.33.
- 2. Lukyanov V.K. JINR E4-94-314, Dubna, 1994.

- 3. Lukyanov V.K. Bull. of Russ. Acad. of Sc., Physics, 1994, 58, p.6.
- Lukyanov V.K. Proc. Int. School-Seminar on HI Phys., Dubna, 1993, v.2, p.129; JINR E7-93-274, Dubna, 1993; Lukyanov V.K., Gridnev K.A., Embulaev A.V. Bull. of Russ. Acad. of Sc., Physics, 1994, 58, p.19.
- 5. Lukyanov V.K., Pol Yu.S. Sov. J. Particles Nucl., 1975, 5, p.385.
- 6. Liguori Neto R. et al. Nucl. Phys., 1993, A.560, p.733.

# EXPERIMENTAL STUDY OF FISSION AND EVAPORATION CROSS SECTIONS FOR <sup>6</sup>He + <sup>209</sup>Bi REACTION

A.S.Fomichev, I.David, Yu.P.Kharitonov, S.M.Lukyanov, Yu.Ts.Oganessian, Yu.E.Penionzhkevich, V.P.Perelygin, N.K.Skobelev, O.B.Tarasov, R.Wolski

Secondary beam of  $^6{\rm He}$  neutron-rich nuclei was produced through a transfer reaction on the carbon target with 35.5 MeV/u  $^7{\rm Li}$  primary beam at the U-400M cyclotron. The influence of the neutron skin of  $^6{\rm He}$  projectile on the fusion-fission and fusion-evaporation cross sections in the reaction with  $^{209}{\rm Bi}$  target was investigated. The  $^{211}{\rm At}$   $\alpha$ -activity following the  $^{209}{\rm Bi}$  ( $^6{\rm He}$ ,  $^4{\rm He}$ ) reaction as well as fission events in the  $^{209}{\rm Bi}$  ( $^6{\rm He}$ ,  $^4{\rm He}$ ) reaction have been recorded by off-line methods. These results are compared with  $^6{\rm He}$  and  $^6{\rm He}$ 0 obtained in the  $^4{\rm He}$ 1 +  $^2{\rm He}$ 20 Bi reaction.

The investigation has been performed at the Flerov Laboratory of Nuclear Reactions, JINR.

Экспериментальное изучение сечений деления и испарения в реакции  $^{6}$ He +  $^{209}$ Bi

# А.С.Фомичев и др.

Вторичный пучок нейтроноизбыточных ядер <sup>6</sup>Не был получен в реакциях передачи на углеродной мишени с использованием пучка  $35.5 \, \mathrm{M9B/hyk}$ лон <sup>7</sup>Li на циклотроне У-400М. Исследовалось влияние нейтронного скина <sup>6</sup>Не на сечения деления и испарения после слияния в реакции на <sup>209</sup>Ві мишени. Альфа-активность ядер <sup>211</sup>А1, возникающих в реакции <sup>209</sup>Ві (<sup>6</sup>Не, 4n), а также осколки деления в реакции <sup>209</sup>Ві (<sup>6</sup>Не, f) регистрировались методом off-line. Эти результаты сравниваются с  $\sigma_{fis}$  и  $\sigma_{4n}$ , полученными в реакции <sup>4</sup>Не + <sup>209</sup>Ві.

Работа выполнена в Лаборатории ядерных реакций им. Флерова ОИЯИ.

#### 1. Motivations

The neutron skin of the nucleus has been one of the central issues of nuclear structure and its existence has remained an open problem for decades. The neutron skin has been studied in detail for stable nuclei with large neutron excess such as <sup>48</sup>Ca and <sup>208</sup>Pb. However no significant difference in the radii between proton and neutron distributions has been observed in these nuclei [1]. It is only recently that the neutron skin for

radioactive neutron-rich nuclei such as <sup>6</sup>He and <sup>8</sup>He has been seen experimentally and a very thick neutron skin was found [1]. The rms radius difference for both nuclei was found about 0.9 fm, but if for <sup>8</sup>He it is not due to the neutron halo (the separation energy of a pair of neutrons is 2.1 MeV), for <sup>6</sup>He it is more arbitrary to say whether it is due to the neutron halo or due to the skin because the separation energy of the last two neutrons is 0.97 MeV. For <sup>6</sup>He radioactive nuclei there appears an interplay between the skin and neutron halo effects at energies around the Coulomb barrier.

The neutron skin is expected to have a prominent effect on nuclear reactions, for instance, the fusion reactions. The neutrons in the skin are expected to have more mobility than neutrons in normal nuclei, because:

- i) A more gradual potential near the surface yields less reflection of incoming waves;
  - ii) A mean free path of a neutron can be longer due to lower density.

The soft dipole mode [2] is expected to occur in nuclei with the neutron skin. Combining the above effects, one can expect that such fast flow of neutrons, which can be viewed as «neutron avalanche», should occur, enhancing the reaction cross section. Takigawa et al. [3] define the fusion cross section as the sum of the incoming particle plus that of the break-up channel, but the role of the break-up channel is very contradictory. Hussein et al. [4] argue that the coupling to the break-up channel would seriously inhibit the total fusion cross section. Dasso and Vitturi in a recent theoretical work [5] have predicted that inclusion of the break-up channel leads always to an enhancement of the fusion cross section at energies close to the Coulomb barrier.

The investigation of the role played by the neutron skin of  $^6$ He and its influence on the fusion cross section in the reaction with  $^{209}$ Bi is the main motivation for this paper. The fusion process has been identified through the detection of the delayed  $\alpha$ -particle emitted by the decay of the ground state of the  $^{211}$ Po obtained from  $\beta$ -decay of  $^{211}$ At evaporation residue populated after a 4n evaporation. Study of the 4n evaporation channel is convenient because the neutron halo and skin have an insignificant overlapping energy region. Moreover, at the same time the fusion-fission cross section for this reaction in a wide energy region was measured, too [6]. Comparing the results of both experiments with the same data for the  $^4$ He +  $^{209}$ Bi reaction one could pin down the neutron skin effect for  $^6$ He nuclei.

### 2. The Experiment

A helium-6 isotope was produced using the primary ion beam of  $^7\text{Li}$  (35.5 MeV/u) at the U-400M cyclotron (FLNR, Dubna). Stripping of a proton from the  $^7\text{Li}$  ions on the 1.1 mm carbon target was used. The intensity of  $^6\text{He}$  measured by a Si(Li) detector with dimensions of  $\varnothing 32 \times 4.15$  mm<sup>2</sup> was about 6000 pps for  $2 \cdot 10^{11}$  pps of  $^7\text{Li}$  ions. The secondary beam purity up to 96% was reached due to the so-called form degrader (1.6 mm Al) positioned between the dipole magnets at the angle of 25° to the beam direction. Additionally, an  $\Delta E$  detector 4150  $\mu$ m in thickness reduced the energy down to 70 MeV±8% (fwhm) at the experimental target position (Fig.1,a).

The  $^{211}$ At( $T_{1/2}=7.22$  h)  $\alpha$ -activity following the  $^{209}$ Bi( $^{6}$ He,  $^{4n}$ ) reaction as well as fission events in the  $^{209}$ Bi( $^{6}$ He,  $^{f}$ ) reaction have been recorded off-line. For fission registering the track detector method was used [7]. Special «sandwich-type» piles consisting of eight  $^{209}$ Bi targets (0.82 mg/cm²),  $55\,\mu$ m-thick mylar films for registration of fission fragments and additional absorbers made of Al ( $60+220\,\mu$ m) were manufactured. Such piles were installed perpendicularly to the incident beam between  $\Delta E-E$  Si(Li) detectors that provided the secondary beam monitoring. The residual energy for  $^{6}$ He ions was 22 MeV±25% (Fig.1b). The counting error provided by the scaler was less than 2% and the losses of ions connected with the absorption inside the targets and aluminium foils and with multiscattering were of the order of 1%. The aluminium foils and bismuth targets were tested for uranium contamination using the neutron-activation method. The analysis showed that it did not exceed  $10^{-7}$  at/at.

This pile was irradiated for 17 hours by a flux of  $^6{\rm He}$  ions with the intensity of  $I\approx 2500$  pps, constant within 10% variation, for the beam diameter of 15 mm. Then the  $\alpha$ -activity of the last four targets, which correspond to the energy range  $E_{cm}\approx 20$ +48 MeV, was simultaneously measured by a low background  $\alpha$ -decay spectrometer [8]. The recording time was longer than  $T_{1/2}$  of  $^{211}{\rm At}$ . The isotope  $^{211}{\rm At}$  undergoes  $\alpha$ -decay (42%,  $E_{\alpha}=5.87$  MeV) and in 58% of the cases goes to the short lived  $(T_{1/2}\sim 0.5~{\rm s})^{211}{\rm Po}$  which in turn undergoes  $\alpha$ -decay with an energy  $E_{\alpha}=7.45$  MeV. Figure 2 shows the total  $\alpha$ -yield for all targets without

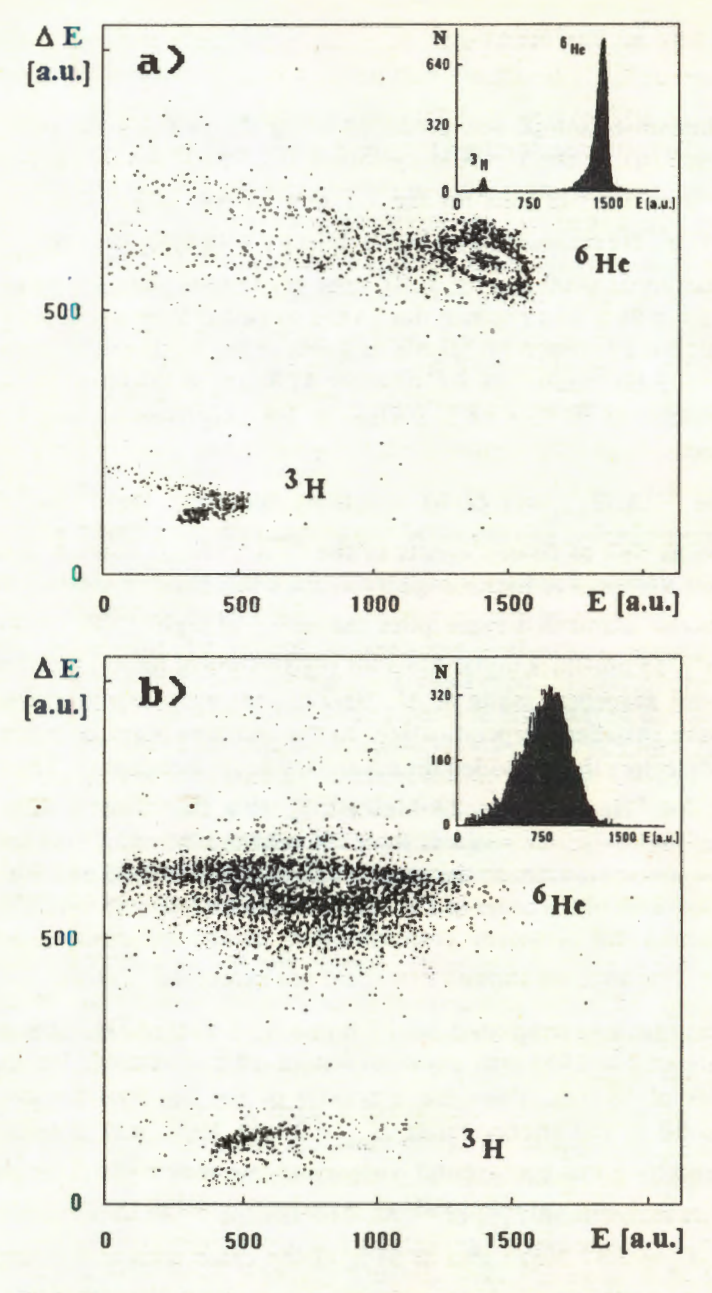


Fig.1. The secondary beam quality obtained without (a) and after (b) going through the pile

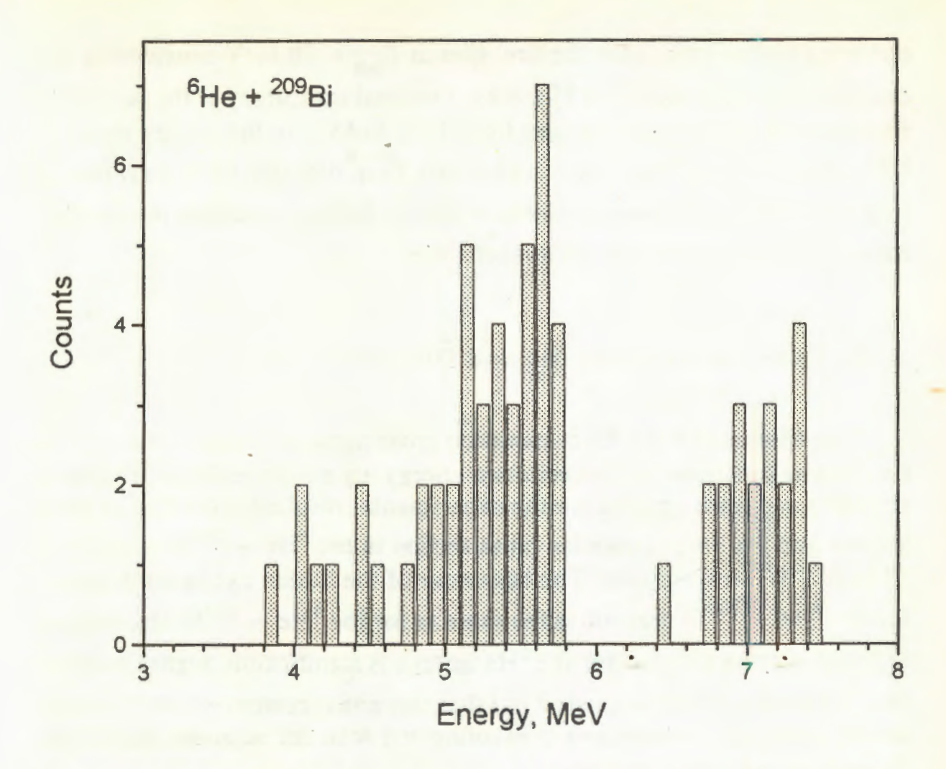


Fig. 2. Alpha energy spectra from the ground state decay of the evaporation residue populated

background subtraction. The first peak ( $E_{\alpha}=5.87$  MeV) belongs to the energy region where other nuclei give their contributions. The second peak ( $E_{\alpha}=7.45$  MeV) with measured half-life of about 7 h corresponds to  $^{211}$ Po and allows good identification of the evaporation residue  $^{211}$ At populated after the 4n evaporation. Moreover in this energy region ( $E_{\alpha}>6$  MeV) only one background event was registered. Unfortunately, we have imperfect information about the  $\sigma_{6n}$  value because of the experimental conditions and the  $\alpha$ -decay properties of the  $^{209}$ At residue ( $T_{1/2}=5.4$  h,  $E_{\alpha}=5.65$  MeV, 5%).

To identify fission fragment events the mylar films were etched in a NaOH solution and scanned under a microscope with 100-200 magnification. For instance, in the  $^6$ He +  $^{209}$ Bi reaction the number of the

observed fission events for the first film at  $E_{\rm lab} = 70$  MeV considering the detector efficiency was  $228 \pm 17$  tracks. The total inaccuracy of the measured fission cross section was changed from 14% to 55% in the energy range of  $^6$ He nucle  $E_{\rm lab} \approx 70 + 30$  MeV. The last film did not have any fission fragment events and one can conclude that the background from the satellite particle  $^3$ H was limited by the level of 1 mb.

# 3. Experimental Results and Discussion

The fission and the 4n evaporation cross sections for the  $^6\mathrm{He}$  +  $^{209}\mathrm{Bi}$  reaction as functions of the excitation energy are shown in Fig.3. The open triangles and open squares are the experimental results for the fission cross section and the 4n evaporation cross section in the  $^4\mathrm{He}$  +  $^{209}\mathrm{Bi}$  reaction in [9] and [10], respectively. The behaviour of the fission excitation function for the  $^6\mathrm{He}$  +  $^{209}\mathrm{Bi}$  reaction is the same as for the  $^4\mathrm{He}$  +  $^{209}\mathrm{Bi}$  reaction but the fission cross section for the  $^6\mathrm{He}$  isotope is significantly higher than for the  $^4\mathrm{He}$  nuclei. It was suggested [6] that this enhancement depends mainly on the entrance channel and it is connected with the neutron skin of the  $^6\mathrm{He}$  nuclei.

The tentative excitation function of the <sup>211</sup>At residue is presented by the solid squares in Fig.3 and the data are listed in the Table:

E <sub>cm</sub> , MeV	$\alpha$ -yeilds ( $E_{\alpha} = 6.75 + 7.45 \text{ MeV}$ )	$\sigma_{4n}$ , mb	
23.6±4.2	6	693±277	
30.4±3.9	8	925±323	
39.0±3.5	5	578±260	
45.8±3.0	4	462±230	

It is clear that the precise position of maximum of  $\sigma_{4n}$  does not follow from this data but one can compare our results with the measured 4n evaporation cross sections for the  $^4\text{He} + ^{209}\text{Bi}$  reaction (open squares) from ref. [10]. The absolute values of  $\sigma_{4n}$  for both reactions agree well within the statistical errors. In the first approximation we can assume that the fission excitation function is more sensitive to  $^6\text{He}$  structure than the evaporation cross

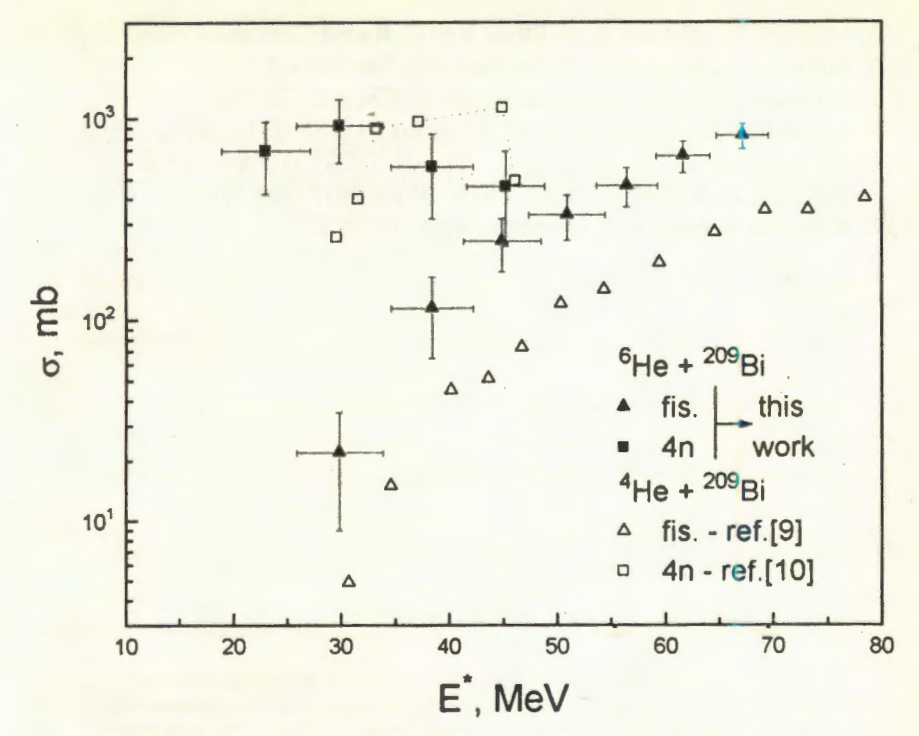


Fig. 3. Fusion-fission ( $\triangle$ ) and 4n evaporation ( $\blacksquare$ ) cross sections in dependence on excitation energy for  $^6\text{He} + ^{209}\text{Bi}$  reaction and fusion excitation functions for  $^4\text{He} + ^{209}\text{Bi}$ : ( $\triangle$ ) — fission, ( $\square$ ) — 4n

sections in the fusion reaction on the  $^{209}$ Bi target. Nevertheless, better statistics are obviously needed for a more detailed analysis. The nearest measurement of the ratio between  $\sigma_{4n}$  and  $\sigma_{6n}$  will also help to confirm our

assumption about the skin effect influence of <sup>6</sup>He on the fusion-evaporation cross sections.

The authors express their gratitude to Dr. N.I.Tarantin for assistance in the experiment. The authors acknowledge the support of the RFBR (Project 93-02-3701).

#### References

- 1. Tanihata I. et al. Phys. Lett., 1992, B289, p.261 and ref therein.
- 2. Tanihata I. Nucl. Phys. 1991, A552, p.275c and ref. therein.
- 3. Takigawa N et al. Phys. Rev., 1993, C47, p.2470.
- 4. Hussein M.S. et al. Phys. Rev., 1992, C46, p.377.

- 5. Dasso C.H., Vitturi A. Phys. Rev C, Rapid Communication, in print.
- 6. Fomichev A.S. et al. Submitted to Z. für Phys.A.
- 7. Ralarosy J. et al. Phys. Rev., 1973, C8, p.2372.
- 8. Kuznetsov A.N. et al. JINR Preprint P13-85-637, Dubna, 1985.
  9. Khodai-Joopari A. Ph. D. Thesis UCRL-16489, Berkley, 1966, A.V.Ignatyuk et al. — Nucl. Phys. (Russian), 1984, V40, p.1404.
- 10. Rattan S.S. et al. Radiochim. Acta, 1992, 57, p.7.

# TENSOR ANALYZING POWER $T_{20}$ FOR $d^{\uparrow} + {}^{12}C \rightarrow p + X$ AT $\Theta_p = 0^{\circ}$ IN THE REGION OF HIGH INTERNAL MOMENTA IN THE DEUTERON\*

E.V.Chernykh, A.A.Nomofilov, V.V.Perelygin, V.I.Sharov, D.A.Smolin, V.N.Sotnikov, L.N.Strunov, S.A.Zaporozhets, A.V.Zarubin, V.E.Zhiltsov, L.S.Zolin

Joint Institute for Nuclear Research, Dubna 141980, Moscow region, Russia

#### A.A.Izotov

St. Petersburg Institute for Nuclear Physics, Gatchina 188350, Russia

T.Aono . T.Hasegawa

Miyazaki University, Faculty of Engineering, Gakuen-Kihanadai, Nishi-1, Miyazaki 889-21, Japan

N.Horikawa, T.Iwata, A.Ogawa, T.Sasaki, S.Toyoda, T.Yamada, Nagoya University, Department of Physics, Furo-Cho, Chikusa-ku, Nagoya 464, Japan

#### T. Dzikowski

University of Lodz, Lodz 91131, Poland

The tensor analyzing power  $T_{20}$  for the reaction  $d^{\dagger} + {}^{12}C \rightarrow p(0^{\circ}) + X$  has been measured in the region of proton internal momenta k in light-cone dynamics up to 1 GeV/c. Measurements have been carried out with Dubna polarized deuteron beam at deuteron momenta up to 9 GeV/c. The results show that as the internal momentum increases the  $T_{20}$  tends to approach the value obtained by the calculation based on the reduced nuclear amplitude method in which the quark degrees of freedom were taken into account.

The investigation has been performed at the Laboratory of High Energies,

Тензорная анализирующая способность  $T_{20}$  для реакции  $d^{\dagger} + {}^{12}\text{C} \rightarrow p + X$  при  $\Theta_p = 0^{\circ}$  в области высоких внутренних импульсов в дейтроне

Черных Е.В. и др.

Тензорная анализирующая  $T_{20}$  способность реакции  $d^{\dagger} + {}^{12}{\rm C} \rightarrow p(0^{\circ}) + X$  измерена в области внутренних импульсов протона k в динамике светового фронта вплоть до 1 ГэВ/с. Измерения были выполнены на пучке поляризованных дейтронов с импульсом до 9 ГэВ/с. Результаты измерений показывают, что по мере роста внутреннего импульса  $T_{20}$  стремится к пределу, полученному в расчетах, основанных на методе редуцированных ядерных амплитуд, учитывающем кварковые степени свободы.

Работа выполнена в Лаборатории высоких энергий ОИЯИ.

<sup>\*</sup>This work was supported by the Russian Fund of the Fundamental Investigations (grant No.93-02-3961) and the Japan Society for the Promotion of Science (JSPS).

The investigation of the deuteron structure at small internucleonic distances high internal momenta) is one of the most interesting subjects in nuclear physics. At that case the wave functions of two nucleons in the deuteron overlap each other largely and the quark-gluon degrees of freedom would be expected to emerge rather than the nucleon-meson degrees of freedom. The internal structure of the deuteron has been studied at short distances in the reactions  $d + A \rightarrow p + X$  at 0° [1-7],  $\gamma d \rightarrow pn$  [8], inelastic [9] and elastic ed scattering at a large angle [10] and dp elastic backward scattering [11]. In particular, in the breakup reaction  $d + A \rightarrow p + X$  it has been studied at the shortest internucleonic distances. So using 8.9 GeV/c unpolarized deuteron beam, the Dubna group [1] measured the cross section of the forward breakup reaction  $d + C \rightarrow p + X$ at the internal momenta in light cone dynamics k up to 1 GeV/c. The momentum spectrum obtained in the experiment was not reproduced by the models using conventional wave functions [12] [13]. On the contrary, the model with hybrid deuteron wave function [1,14] which includes a small amount of six-quark admixture described the data satisfactorily. This model also described T20 data obtained in the experiments at Saclay [2] and Dubna [3]. In accordance with maximum deuteron beam momenta available at Saclay (3.5 GeV/c) and Dubna (9.1 GeV/c) the breakup deuteron reaction can be studied up to internal momenta k about 0.54 GeV/c and 1.04 GeV/c, respectively. The first measurements of T<sub>20</sub> performed at Dubna by ALPHA group [3] contained fairly large errors at k higher than 700 MeV/c. Recently new measurements of T20 have been performed by the ANOMALON group at Dubna with smaller errors [4].  $T_{20}$  up to k = 825 MeV/c found to be still negative and more similar to the QCD prediction than to the calculations with conventional wave functions. However, a crucial test should be made at higher internal momenta where the calculations with conventional wave functions give considerably different values of T20 against the QCD prediction.

Another important spin observable in the breakup reaction is the polarization transfer coefficient  $\kappa_0$ ;  $\kappa_0 = V_p/V_d$  where  $V_p$  is the polarization of the emitted proton and  $V_d$  is the vector polarization of the deuteron. This observable has been measured in the region of internal momenta k up to 550 MeV/c [5—7], where its value has turned close to zero that contradicts the predictions of NN-potential models at the impulse approximation approach. For more complete information on the deuteron wave function at small internucleonic distances, further polarization experiments have been required.

In this paper we report the results of tensor analyzing power T<sub>20</sub> measurement for the reaction  $d^{\uparrow} + {}^{12}C \rightarrow p + X$  by detecting the protons emitted at the forward angles  $\Theta_p \le 1.3^\circ$  at deuteron momenta from 6.0 GeV/c to 9.0 GeV/c. The experiment was performed at the Synchrophasotron of the Joint Institute for Nuclear Research using tensor polarized deuteron beam provided by POLARIS ion source [15]. POLARIS possesses ability to operate either in the vector polarization mode or the tensor polarization one and repeat pulse by pulse any combination in three polarization states «+», «0», «-» where «+» and «-» denote positive and negative polarization states and «0» denotes unpolarized state. A negligible depolarization at the Synchrophasotron was confirmed experimentally in the vector polarization mode [16]. For T20 data taking we used «+» and «-» polarization states in the tensor polarization mode. Typical beam intensity was ~2·109 deuterons/pulse. The values of the deuteron beam polarization components were measured by detecting dp elastic scattering at 3 GeV/c with the fast two arm beam line polarimeter ALPHA [16]. The polarization measurement was carried out before and after the measurement of T20 and it was confirmed that the beam polarization remained stable. The T20 measurements under the same kinematic conditions were repeated with intervals of several hours. Reproduction of the values of T20 gives another confirmation of deuteron polarization stability within the measurement time. The tensor and admixture vector polarizations of the beam were

$$p_{zz}^{+} = +0.543\pm0.013$$
(stat.)  $\pm0.022$ (syst.),  
 $p_{z}^{+} = 0.222\pm0.007$ (stat.)  $\pm0.004$ (syst.)

for «+» polarization state and

$$p_{zz}^{-} = -0.709 \pm 0.013 \text{(stat.)} \pm 0.028 \text{(syst.)},$$
  
$$p_{z}^{-} = 0.200 \pm 0.010 \text{(stat.)} \pm 0.004 \text{(syst.)}$$

for «-» polarization state. To estimate the systematical errors for measured  $p_z$  and  $p_{zz}$  values we took total uncertainties for the known dp elastic scattering analyzing powers  $A_y$  and  $A_{yy}$  [17].  $T_{20}$  for the reaction  $d^{\dagger} + {}^{12}\text{C} \rightarrow p(0^{\circ}) + X$  is derived from the differential cross section defined by the formulae,

$$\sigma^{\pm} = \sigma^{0} \left( 1 - \frac{1}{2} \rho_{20}^{\pm} T_{20} \right), \tag{1}$$

where  $\sigma^+$  and  $\sigma^-$  are the cross sections for positive (+) and negative (-) aligned beams,  $\sigma^0$  is that for an unpolarized beam and  $\rho_{20} = p_{zz} / \sqrt{2}$  is the beam alignment in spherical form. Then  $T_{20}$  is reduced to

$$T_{20} = \frac{2(n^+ - n^-)}{n^+ \rho_{20}^- - n^- \rho_{20}^+},$$
 (2)

where  $n^+$  and  $n^-$  are counts of the detected protons normalized by the deuteron beam intensities for positive (+) and negative (-) alignments. The experiment has been performed at 4.5, 6.5 and 7.5 GeV/c of beam line momenta for the emitted protons. To vary the internal momentum k at fixed beam line momentum we changed the momentum of the incident deuterons.

Table 1. Kinematic conditions of data taking

	T				
No.	P <sub>d</sub> (GeV/c)	P <sub>L</sub> (GeV/c)	k <sub>11</sub> (GeV/c)	q <sub>11</sub> (GeV/c)	
1	9.00	7.50	0.814	0.493	
2	8.90	7.50	0.855	0.505	
3	8.70	7.50	0.949	0.528	
4	9.00	6.50	0.455	0.347	
5	8.41	6.50	0.600	0.416	
6	8.00	6.50	0.725	0.464	
7	7.80	6.50	0.806	0.497	
8	9.00	4.50	0.000	0.000	
9	6.85	4.50	0.299	0.252	
10	5.97	4.50	0.524	0.382	

Table 1 shows the set of kinematical conditions, under which we took the data: these are incident deuteron momentum  $P_d$  and beam line momentum  $P_L$ . Corresponding values of internal momentum  $k_{\parallel \parallel}$  and momentum of proton in the deuteron rest frame  $q_{\parallel \parallel}$  are also given in Table 1. The longitudinal component of q is obtained by the Lorentz transformation of the laboratory proton momentum:

$$q_{\perp \perp} = \gamma (P_{\perp \perp} - \beta E_p) \tag{3}$$

with  $\gamma = E_d / m_d$  and  $\gamma \beta = P_d / m_d$ , where  $P_{++} = P_p \cos \Theta_p \sim P_p$ ;  $P_p$  and  $E_p$ ,  $P_d$  and  $E_d$  are the momenta and energies of proton and deuteron, respectively. The momentum k called internal momentum in light-cone dynamics is expressed by the following formula (see [14] and other references therein)

$$k^2 = \frac{m_{\perp}^2}{4\alpha (1 - \alpha)} - m_p^2 \tag{4}$$

with  $m_{\perp}^2 = k_{\perp}^2 + m_p^2$ , where  $k_{\perp}$  is the transverse momentum of the proton. The light-cone variable  $\alpha$  [18] is the part of the deuteron momentum carried by the proton in the infinite momentum frame and is expressed by  $\alpha = (E_p + P_p)/(E_d + P_d)$ . When the light-cone variable  $\alpha$  is not close to 1/2, the transverse momentum  $k_{\perp}$  (~0.04 GeV/c) can be neglected and then  $k^2$  is reduced to

$$k^2 \cong \frac{m_p^2}{4\alpha (1-\alpha)} - m_p^2. \tag{5}$$

This expression was used in the analysis except the point at  $k \cong 0$ , where k was calculated by equation (4) with  $k_{\perp} = 44$  MeV/c as the mean weighted value of  $k_{\perp}$  estimated by the acceptance at the focus F3.

The stripping reaction  $d^{\uparrow} + ^{12}\text{C} \rightarrow p + X$  occurred in a carbon target located at the beam line focus F3 (see Fig.1). The target was 30 cm (50 g/cm²) along the beam and 6 cm across while the beam spot at F3 did not exceed 3 cm. The beam position at F3 was under control by the multiwire ionization beam profilemeter and was found stable within  $\pm 1$  mm in the data taking time. The quadrupole magnet located 4.5 m downstream F3 accepted the particles emitted at angle  $\Theta_p \leq 1.3^\circ$ . The beam line consisting of bending magnets B1—B3 and quadrupole magnets selected the particles having the required momentum; the momentum bite of the beam line was  $\pm 2\%$ . For particle identification, the two independent TOF counter systems were used. The TOF counters were placed at F4 ( $S_{\text{TOF1}}$ ), F5 ( $S_{\text{TOF2}}$ ) and F7( $S_{\text{TOF3}}$ ). The particles having passed through the beam line were detected by the magnetic spectrometer ANOMALON [19] located at F7. The spectrometer (Fig.1) was composed of an analyzing magnet (SP-40) and 9 MWPCs with a wire spacing of 1mm (PC3-5) and 2mm (PC1,2,6—9).

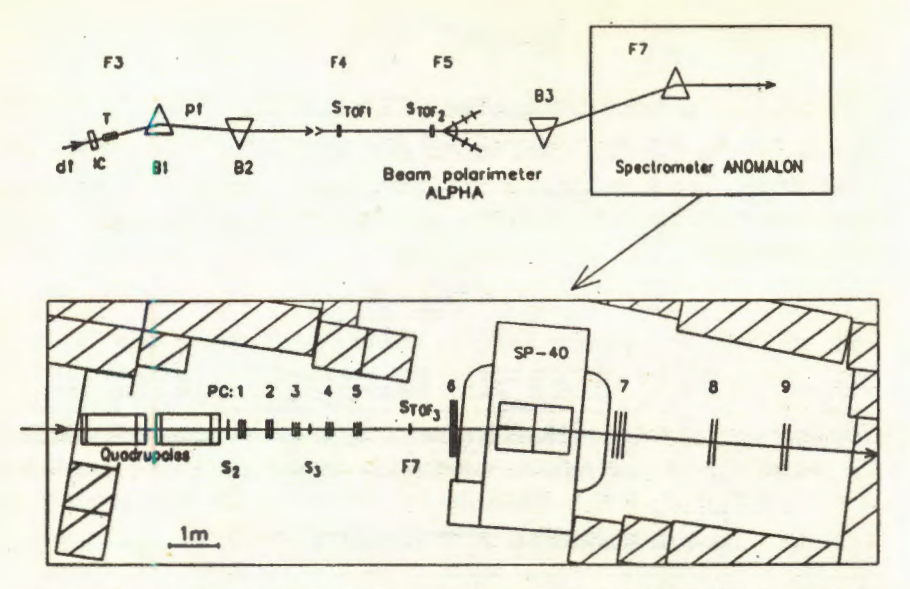


Fig.1. Schematic layout of the beam line and the spectrometer ANOMALON. B denotes the bending magnets. F3, F4, F5 and F7 are the focusing points

The first 7 MWPCs had 3 planes (X, U, V) and the two last ones (PC8,9) had 2 planes (X, Y). A momentum resolution of spectrometer was equal to 0.76% for 7.5 GeV/c protons. The deuteron beam intensity was measured by an ionization chamber (IC) placed in front of the carbon target (see Fig.1).

The event trigger logic of data acquisition was made according to

$$(N1 \cdot M1 \cdot S2 \cdot S3) \cdot (TX1 \cdot TX2).$$

N1, M1, S2 and S3 were trigger counters located at F7, four-fold N1·M1·S2·S3 coincidences formed a beam particle signal. All trigger and TOF counters were made of plastic scintillators 8 to 10 mm thick. TX1 and TX2 were TOF counters using Phillips XP2020 photomultipliers: the former was located at F4 and the latter at F7. These TOF counters were used to suppress the deuteron events at the stage of fast trigger. To select the proton events the final particle identification was carried out by another TOF counter system using Hamamatsu photomultipliers (H2431): the start timing signal of TDC was fed from TOF counter N1 located at F7, and the stop timing signals were sent from two TOF counters N2 at F4 and M2 at F5. This system gave us two TOF timings: one was between F4 and F7 (~70 m) called T2 and the other was between F5 and F7 (~45 m) called T3. In the off-line analysis the correlation of T2 and T3 was examined and the

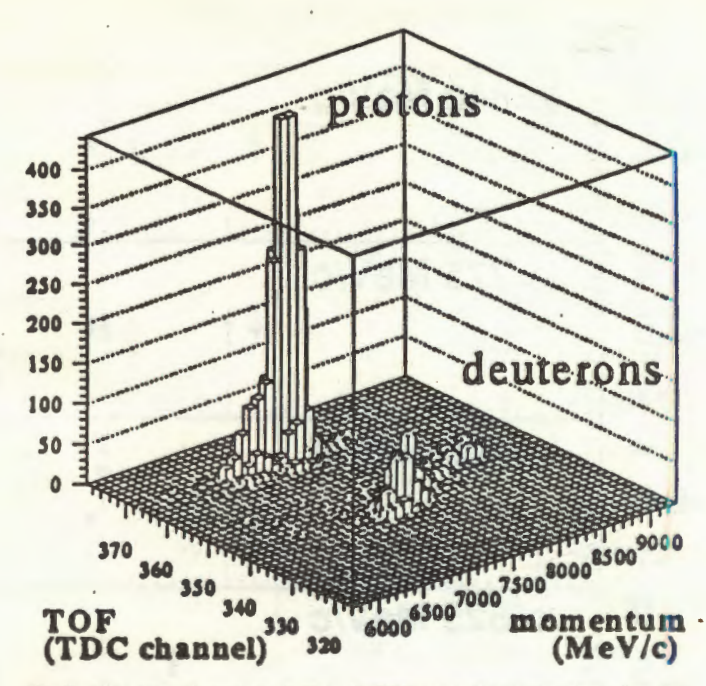


Fig. 2. The two-dimensional plot of TOF and the momentum for the detected events of data set No.3 (Table 1). In the TOF time scale one digit of TDC corresponds to 220 ps/channel

uncorrelated events were discarded. A typical two-dimensional plot of TOF (T2) and the momentum for the events having passed through the correlation check is shown in Fig.2 for data set No.3 in Table 1. As one can see protons are clearly separated from the deuterons.

Dividing the events of each set of data typically into three to five bins of k with bites of 50 to 80 MeV/c, we derived the  $T_{20}$  values. The  $T_{20}$  values of the same k bins but for different deuteron beam momentum  $P_d$  are displayed in Fig.3. One can conclude that there is no indication of that  $T_{20}$  depends on  $P_d$ . The events for the same k bins were combined and the  $T_{20}$  values were calculated. The combined  $T_{20}$  values are shown in Table 2 as a function of k, q and  $\alpha$ . The indicated systematic errors are dominantly originated from uncertainty of the analyzing power of elastic dp scattering [17]. The obtained values of  $T_{20}$  are plotted in Fig.4 with the data of other groups and theoretical calculations. In the region where other group's data and ours overlap, the data are in good agreement with each other. Our data in the

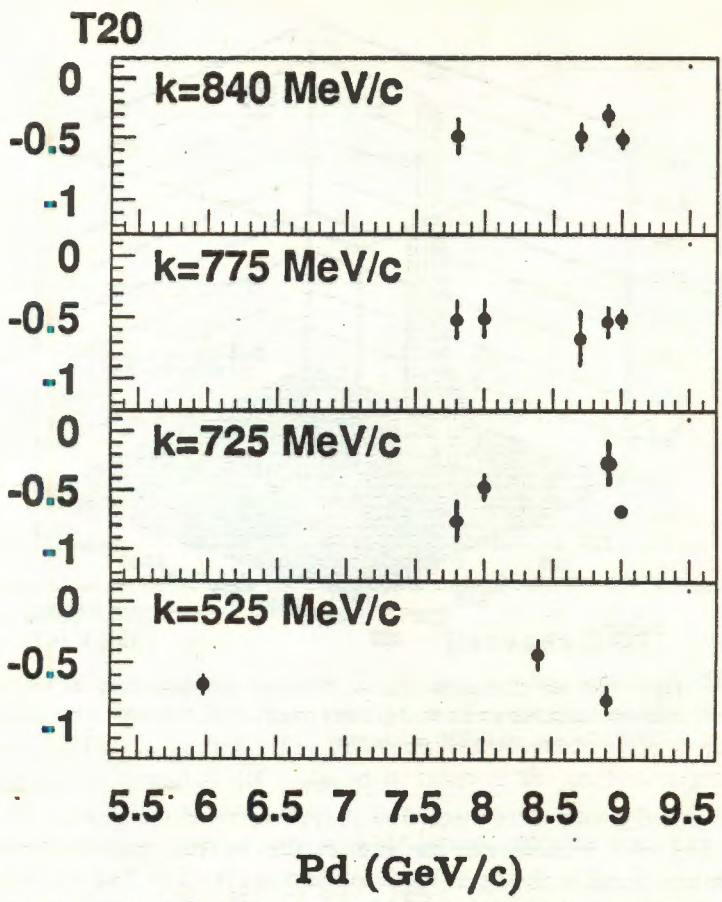


Fig. 3.  ${\bf T}_{20}$  for the same k bins at different deuteron beam momenta  $P_d$  . The errors bars display statistical errors

high internal momentum region, k > 850 MeV/c, show a tendency of approaching of  $T_{20}$  to the QCD motivated asymptotic prediction  $(T_{20} \rightarrow -0.3)$  [20] based on the reduced nuclear amplitude (RNA) method [21], as the arrow with the dashed line 5 in Fig.4 shows. Curves 1, 2 and 3 are the results of the calculation [22] by relativistic treatment using conventional wave functions: 1— spectator mechanism (SM) with the Reid soft core wave function, 2—SM including final state interaction (FSI) with the Reid soft core wave function, 3—SM including final state interaction with the Paris wave function. They indicate the change of the sign of  $T_{20}$  at

Table 2.  $T_{20}$  as a function of k, q and  $\alpha$ 

k (MeV/c)	åk (MeV/c)	q (MeV/c)	а	$T_{20} \pm \text{stat.} \pm \text{sys.}$ $-0.083 \pm 0.027 \pm 0.003$	
47	7	47	0.500		
. 275	10	235	0.640	$-0.833\pm0.057\pm0.033$	
325	11	269	0.664	$-0.810\pm0.047\pm0.032$	
375	12	301	0.686	$-0.790\pm0.072\pm0.032$	
425	13	330	0.706	$-0.600\pm0.056\pm0.024$	
475	14	358	0.726	-0.583±0.049±0.023	
525	15	383	0.744	$-0.663\pm0.053\pm0.027$	
575	17	406	0.761	$-0.572\pm0.060\pm0.023$	
625	19	427	0.777	$-0.506\pm0.062\pm0.020$	
675	21	447	0.792	-0.570±0.093±0.023	
725	23	465	0.806	-0.601±0.057±0.024	
775	25	481	0.818	-0.520±0.053±0.02	
840	29	500	0.833	-0.453±0.048±0.018	
920	35	521	0.850	-0.400±0.063±0.010	
1000	38	539	0.864	-0.351±0.116±0.01	

&k denotes uncertainty of k due to our momentum resolution for breakup protons

k below 950 MeV/c. On the contrary, our results show that  $T_{20}$  still remains negative even at k=1000 MeV/c. Curve 4 is the result of the calculation with allowance for the composite 6-quark component [23].

To conclude: we have measured the tensor analyzing power  $T_{20}$  for the reaction  $d^{\uparrow} + {}^{12}\text{C} \rightarrow p(0^{\circ}) + X$  in the region of proton internal momenta of light-cone dynamics up to 1 GeV/c. The results have shown a tendency that  $T_{20}$  is approaching the asymptotic prediction  $(T_{20} \rightarrow -0.3)$  obtained in the calculation based on the reduced nuclear amplitude method in which the quark degrees of freedom are taken into account.

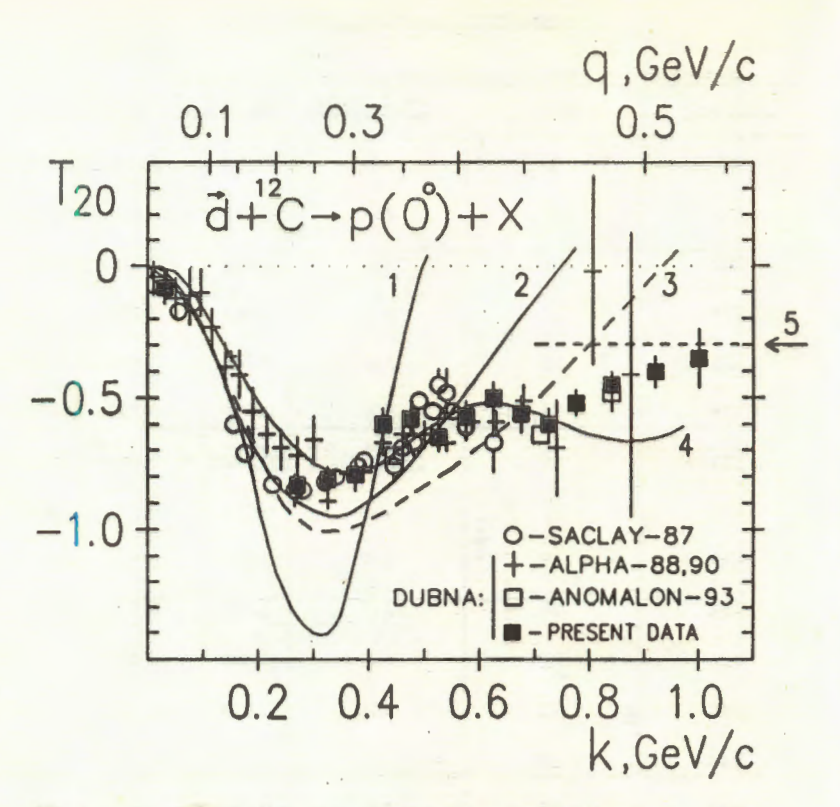


Fig. 4.  $T_{20}$  as a function of k and q. Hatched squares are the present results. Open circles are from [2]. Crosses and open squares are Dubna data from [3] and [4], respectively. The errors are statistical. The curves and arrow are explained in the text

# Acknowledgments

We would like to thank the staff of the engineering departments at LHE, JINR for maintaining the polarized deuteron beam running in good condition and Prof.I.Golutvin and Dr.V.Khabarov for their kind attention and support of our activity. We appreciate assistance of many who provided a technical support of these measurements among whom are A.Litvinenko, A.Khrenov, Z.Motina and P.Kulinich. We thank directorates of JINR and LHE, JINR for a manifold support of this experiment.

## References

- 1. Ableev V.G. et al. Nucl. Phys., 1983, A393, p.491; A411, p.541E.
- 2. Perdrisat C.F. et al. Phys. Rev. Lett., 1987, 59, p.2840.
- 3. Ableev V.G. et al. JETP Lett., 1988, 47, p.649; JINR Rapid Communications No.4 [43]-90, Dubna, 1990, p.5.
- 4. Nomofilov A.A. et al. Phys. Lett., 1994, B325, p.327.
- 5. Cheung E. et al. Phys. Lett., 1992, B284, p.210.
- 6. Atanasov I. et al. In: Proc. of the 10th Intern. Symposium on High Energy Spin Physics, Nagoya, Japan, November 1992 (Universal Academy Press, Inc. Tokyo, Japan), edited by T.Hasegawa, N.Horikawa, A.Masaike and S.Sawada, p.537.
- 7. Golutvin I.A. et al. Proc. of the 10th Intern. Symposium on High Energy Spin Physics Nagoya, Japan, November 1992 (Universal Academy Press, Inc. Tokyo, Japan) edited by T.Hasegawa, N.Horikawa, A.Masaike and S.Sawada, p.501.
- 8. Freedman S.J. et al. Phys. Rev., 1993, C48, p.1864.
- 9. Bosted P. et al. Phys. Rev. Lett., 1982, 49, p.1380.
- 10. The I. et al. Phys. Rev. Lett., 1991, 67, p.173.
- 11. Arvieux J. et al. Nucl. Phys., 1984, A 431, p.613.
- 12. Lacombe M. et al. Phys. Lett., 1981, B101, p.139.
- 13. Reid R.V. Ann. Phys., 1968, 50, p.411.
- 14. Kobushkin A.P., Vizireva L. J. Phys. G.: Nucl. Phys., 1982, 8, p.893.
- 15. Belushkina A.A. et al. In: Proceedings of the 7th Intern. Symposium on High-Energy Spin Physics, vol.2, Provino, 1986, p.215.
- 16. Ableev V.G. et al. Nucl. Instr. and Meth., 1991, A306, p.73.
- 17. Ghazikhanian V. et al. Phys. Rev., 1991, C43, p.1532.
- 18. Dirac P.A.M. Rev. Mod. Phys., 1949, 21, p.392.
- 19. Borsunov Yu.T. et al. In: Proceeding of the International Workshop «Dubna Deuteron-91», Dubna, June 11—13, 1991, JINR, E2-92-25, Dubna 1992, p.185—187.
- 20. Kobushkin A.P. J. Phys. G: Nucl. Part. Phys., 1993, 19, p.1993.
- 21. Brodsky S.J., Hiller J.R. Preprint SLAC-PUB-5763, 1992; Brodsky S.J., Hiller J.R. Phys. Rev., 1983, C28, p.475.
- 22. Lykasov G.I. Phys. Part. Nucl., 1993, 24, p.59.
- 23. Dolidze M.G., Lykasov G.I. Z. Phys., 1990, A335, p.95; Z. Phys., 1990, A336, p.339.

Received by Publishing Department on September 21, 1994.

### THE NUCLOTRON INTERNAL TARGETS\*

## A.S. Artiomov

The peculiarities of the nucleus-internal target interaction at the synchrotrons are theoretically investigated. Taking this interaction into account, analytical expressions for luminosities averaged over cycle time, time evolution of the current, transverse and longitudinal emittances are obtained. The graphical functions, characterizing the luminosities and parameter evolution of a d, C and Ar nucleus beam with energies of 1 and 6 AGeV for different internal targets at the Nuclotron are presented.

The investigation has been performed at the Laboratory of High Energies, JINR

## Внутренние мишени в нуклотроне

## А.С.Артемов

Теоретически исследованы особенности взаимодействия ядер с внутренними мишенями в синхротронах. С учетом этого взаимодействия получены аналитические выражения для усредненных за время цикла светимостей, временной эволюции тока пучка, его поперечного и продольного эмиттансов. Графические зависимости, характеризующие светимости и эволюцию параметров пучка ядер d, C и Ar с энергиями 1 и 6 АГэВ, представлены для различных внутренних мишений в нуклотроне.

Работа выполнена в Лаборатории высоких энергий ОИЯИ.

## 1. Introduction

Relativistic nuclear physics deals with the study of processes in which the constituents of nuclear matter move with relative velocities close to the velocity of light. The asymptotic character of such natural phenomena has played a decisive role in a construction of the Nuclotron, a strong superconducting accelerator of relativistic nuclei at the LHE of the Joint Institute for Nuclear Research in Dubna [1]. As the first experiments [2,3] showed, this accelerator provides good possibilities for internal target technique. The planning of internal target experiments requires a detailed knowledge of the

<sup>\*</sup>Report at the Workshop on Perspectives of Relativistic Nuclear Physics, May 31 — June 5, 1994, Varna, Bulgaria

ion-target interaction. This interaction is sufficiently well studied for the light ion beams circulating into the synchrotrons (see, for example, [4-7]). As shown in this report, for more heavy ions some peculiarities of the ion-internal target interaction take place. Taking this interaction into account, the luminosities averaged over cycle time and parameter evolution of d, C and Ar nucleus beam with energies of 1 and 6 AGeV for different internal targets at the Nuclotron are investigated.

# Beam-Internal Target Interaction at the Synchrotrons and Evolution of an Ion Beam Parameters

Physics experiments with internal targets are usually realized in recirculation mode of synchrotron operation after beam injection and acceleration. It is important for this mode of operation that the mean energy loss of ions per target traversal is compensated by an appropriate synchrotron acceleration in the rf-cavity. If we suppose that ions traverse a homogeneous target every turn and residual gas effects are negligible, general analytical expressions for beam parameter evolution can be obtained.

Small angle scattering and energy loss straggling of ions lead to the growth of transverse and longitudinal beam emittances. For a sufficiently large number of target traversals it can be described by the following equation [7,8]

$$\varepsilon_{i}^{(N)}(\eta) = \varepsilon_{i}^{(0)} + 0.5N\beta_{i}\eta^{2} \overline{(\delta Y')^{2}} + + 0.5N\eta^{2} [\gamma_{i}D_{i}^{2} + 2\alpha_{i}D_{i}D_{i}' + \beta_{i}(D_{i}')^{2}] \overline{\delta^{2}},$$
(1)

$$\varepsilon_l^{(N)}(\eta) = \varepsilon_l^{(0)} + 0.5N\beta \, \eta^2 \delta^2. \tag{2}$$

Here  $\varepsilon_i^{(0)}$ ,  $\varepsilon_i^{(N)}$  are the initial and after N target traversals horizontal (i=x) or vertical (i=z) transverse emittances corresponding to  $\eta$  standard deviations in the Gaussian distribution;  $\varepsilon_l^{(0)}$  and  $\varepsilon_l^{(N)}$  are analogous longitudinal emittances;  $\beta_i$ ,  $\alpha_i$ ,  $D_i$ ,  $D_i'$ ,  $\gamma_i = (1+\alpha_i^2)/\beta_i$  are the parameters of the accelerator at the target location;  $(\delta Y')^2$  and  $\delta^2$  are the mean square deviations in angle and relative momentum after target traversal;  $\beta_l = (\omega_{rf}/\omega_s) \times \sqrt{(|\xi| 2\pi p \beta c)/(ZU \cos \varphi_s)}$ ;  $\omega_{rf}$  and  $\omega_s$  are the frequences of rf-cavity and synchronous particle turn, respectively;  $\xi = \delta (\Delta \omega/\omega)$  is the longitudinal

dispersion of the accelerator; U is the voltage amplitude of rf-cavity;  $\varphi_s$  is the phase of the synchronous particle; p,  $\beta c$  and Z are the momentum, velocity and charge number of ions respectively. Using Moliere's approximation of the screened coulomb potential of the Thomas-Fermi atom and the Landau-like energy loss distribution, for relativistic nuclear-thin target interaction we obtain

$$\overline{(\delta Y')^2} \approx 2 \cdot 10^{-7} t A_0^{-1} \left( \frac{ZZ_0}{A \gamma \beta^2} \right)^2 \left( \ln \left( \frac{\theta_{cm}}{\theta_m} \right) - 0.5 \right) =$$

$$= t \cdot f_1(Z, A, Z_0, A_0, \beta), \tag{3}$$

$$\overline{\delta^2} \approx 2 \cdot 10^{-7} t \frac{Z_0}{A_0} \left( \frac{Z}{\beta^2 A} \right)^2 \left( 1 - \frac{\beta^2}{2} \right) = t \cdot f_2(Z, A, Z_0, A_0, \beta). \tag{4}$$

Here  $\gamma=(1-\beta^2)^{-0.5}$ ; t is the target thickness [g/cm²]; A,  $Z_0$  and  $A_0$  are the nuclear mass number, charge and mass number of the target, respectively;  $\theta_m \approx 4.8 \cdot 10^{-6} \, Z_0^{1/3} \, \sqrt{1+1.77\cdot 10^{-4} (ZZ_0/\beta)^2}/(\beta\gamma A)$  is Moliere's screening angle;  $\theta_{cm} \approx 0.15 \, [1+1.53\cdot 10^{-2} (ZZ_0/\beta)] \cdot [\beta\gamma A(A^{1/3}+A_0^{1/3})]^{-1}$  is the maximum angle of the Rutherford scattering determined by the nuclear radii of target and projectile. As an example, Fig.1 shows the  $f_1()$  and  $f_2()$  curves characterizing the transverse emittance growth of the d, C and

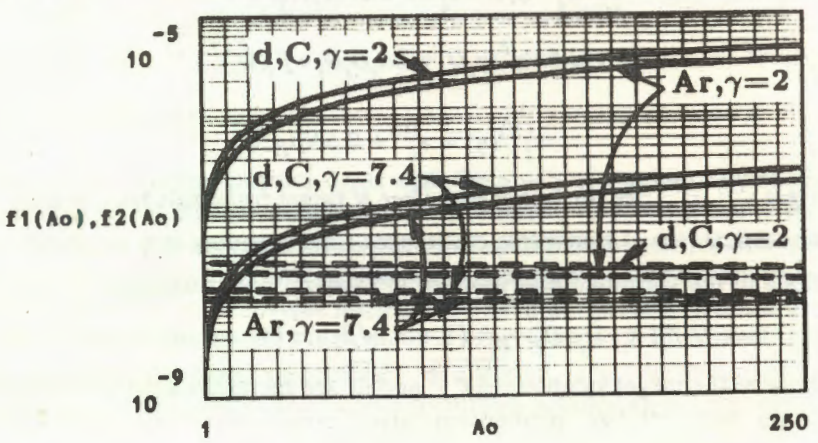


Fig.1. The  $f_1$  (solid line) and  $f_2$  (dashed line) functions vs target mass number  $A_0$  for different incident nuclei

Ar nucleus beam with  $\gamma=2$  and 7.4 for different internal targets. The growth of beam emittances, inelastic nuclear scattering and large angle elastic scattering in a single projectile passage through the target lead to beam losses. If we take into account only the first channel, the time evolution for circulating beam intensity (in relative units) can be obtained from the Fokker-Planck model of projectile diffustion in the  $(Y_i', Y_i)$ -phase spaces [9]. As the longitudinal emittance growth can be influenced by the rf-cavity voltage (see eq.(2)), we suppose that particle losses in the longitudinal phase space can be made negligible. Using the results of ref.[10], the probability of projectile loss because of diffusion in a beam after N target traversals is estimated by  $P(N) = \prod_{i=x,z} P_i(\varepsilon_i^{(N)})$ , where calculated  $P_i(\varepsilon_i^{(N)})$ -function is shown

in Fig.2. Approximating this function by exp  $[-5.36(s_i - 0.06)]$ , the effective cross section  $\sigma_i$  of projectile loss after start time  $\tau_i$  can be obtained as

$$\sigma_{i} \approx 2.2 \cdot 10^{-24} \frac{A_{0}}{A_{i}} \left[ \beta_{i} f_{1}() + f_{2}() \left( \gamma_{i} D_{i}^{2} + 2\alpha_{i} D_{i} D_{i}' + \beta_{i} (D_{i}')^{2} \right],$$
 (5)
$$\tau_{i} \approx \frac{2S \left( 0.12 A_{i} \eta^{2} - \varepsilon_{i}^{(0)} \right)}{t \eta^{2} \beta c} \times$$

$$\times \left[ \beta_{i} f_{1}() + f_{2}() \left( \gamma_{i} D_{i}^{2} + 2\alpha_{i} D_{i} D_{i}' + \beta_{i} (D_{i}')^{2} \right) \right]^{-1} \equiv \frac{S}{t \beta c} ai(),$$
 (6)

where S, A, are the ring circumference and acceptance.

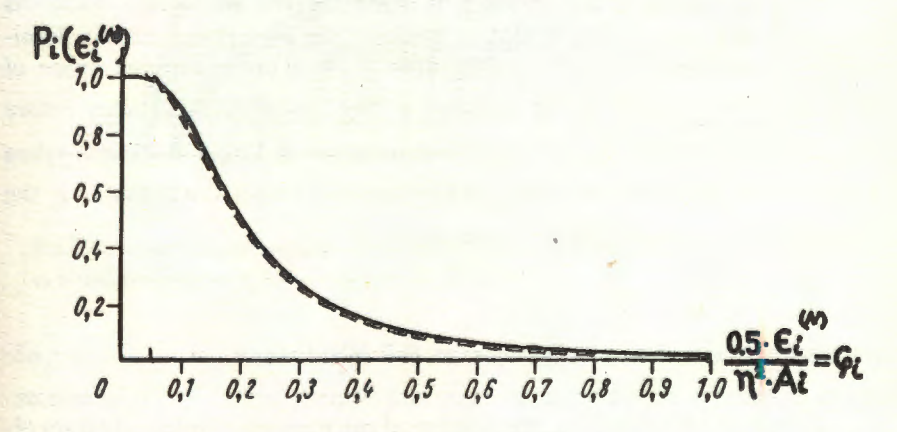


Fig.2. The probability of diffusion particle loss in  $(Y_i, Y_i)$ -phase space for the beam with transverse emittance  $s_i^{(N)}$ , the dashed line shows the exp  $[-5.36(s_i - 0.06)]$  approximation

Inelastic nuclear interaction and large angle elastic scattering lead to the projectile loss in every passage through the target with the cross section

$$\sigma_t = \sigma_c f() + 0.5\sigma_{in} \left[ 4 - er f(\theta_{xa}/2\theta_d) - er f(\theta_{za}/2\theta_d) \right]. \tag{7}$$

Here  $f(\cdot) \equiv 0.5 \ (\theta_{xa}^{-2} + \theta_{za}^{-2} - 2\theta_{cm}^{-2}), \quad \theta_{ia}^2 \approx A_i/(\beta_i\pi) \ (i=x,z), \quad \theta_d \approx 0.15 \ [A(\gamma^2-1)^{0.5} \ (A^{1/3} + A_0^{1/3}) \ ]^{-1}, \quad \sigma_{in} \approx 6 \cdot 10^{-26} (A^{1/3} + A_0^{1/3})^2, \quad \sigma_c \approx 3 \cdot 10^{-31} \ [Z_0 Z/(\beta^2 \gamma A) \ ]^2$  and Gaussian approximation of a central maximum of plane diffractional nuclear scattering is used. In eq.(7) we should assume  $\theta_{ia} = \theta_{cm}$ , when  $\theta_{ia} > \theta_{cm}$ . Depending on the collision energy and the type of colliding nuclei, different terms dominate in  $\sigma_t$ . The average beam lifetime  $(T_b)$  and cross section of the projectile loss  $(\sigma_{loss})$  can be estimated as

$$T_b \approx \frac{a + \sum_{i} \tau_i \sigma_i b_i}{\sigma_i + \sum_{i} b_i \sigma_i}, \quad (i = x, z),$$
 (8)

$$\sigma_{loss} = \sigma_t + \sigma_{ef} = a/T_b, \tag{9}$$

where  $a = A_0 S/(6 \cdot 10^{23} t \beta c)$ ,  $b_i = 1$  if  $\tau_i < T = a/\sigma_t \equiv \overline{t}()$   $S/(t \beta c)$  and  $b_i = 0$  otherwise,  $\sigma_{ef}$  is the effective cross section of the diffusion projectile loss.

The luminosity is the product of beam current and target thickness averaged over time. In recirculation mode of the accelerator run the luminosity  $L_c$  averaged over the cycle time  $T_c$  has the maximum value of  $L_c = N_0/(T_c\sigma_{\rm loss})$  ( $N_0$  is the number of the circulating particles before beam-target interaction) which is independent of target thickness when  $t \ge t_c = A_0 S/(6 \cdot 10^{23} \, T_c \, \beta c\sigma_{\rm loss})$ . For internal target thickness  $t < t_c$  the luminosity is decreased by the value of  $t/t_c$ .

# 3. Internal Target Effects at the Nuclotron

Using the above results, the numerical calculations of internal target effects for d, C and Ar nuclei with energies of 1 and 6 AGeV are obtained at the Nuclotron  $A_i \approx 40\pi$  mm·mrad,  $\varepsilon_i^{(0)} \approx 2\pi$  mm·mrad,  $\beta_i \approx 780$  cm,

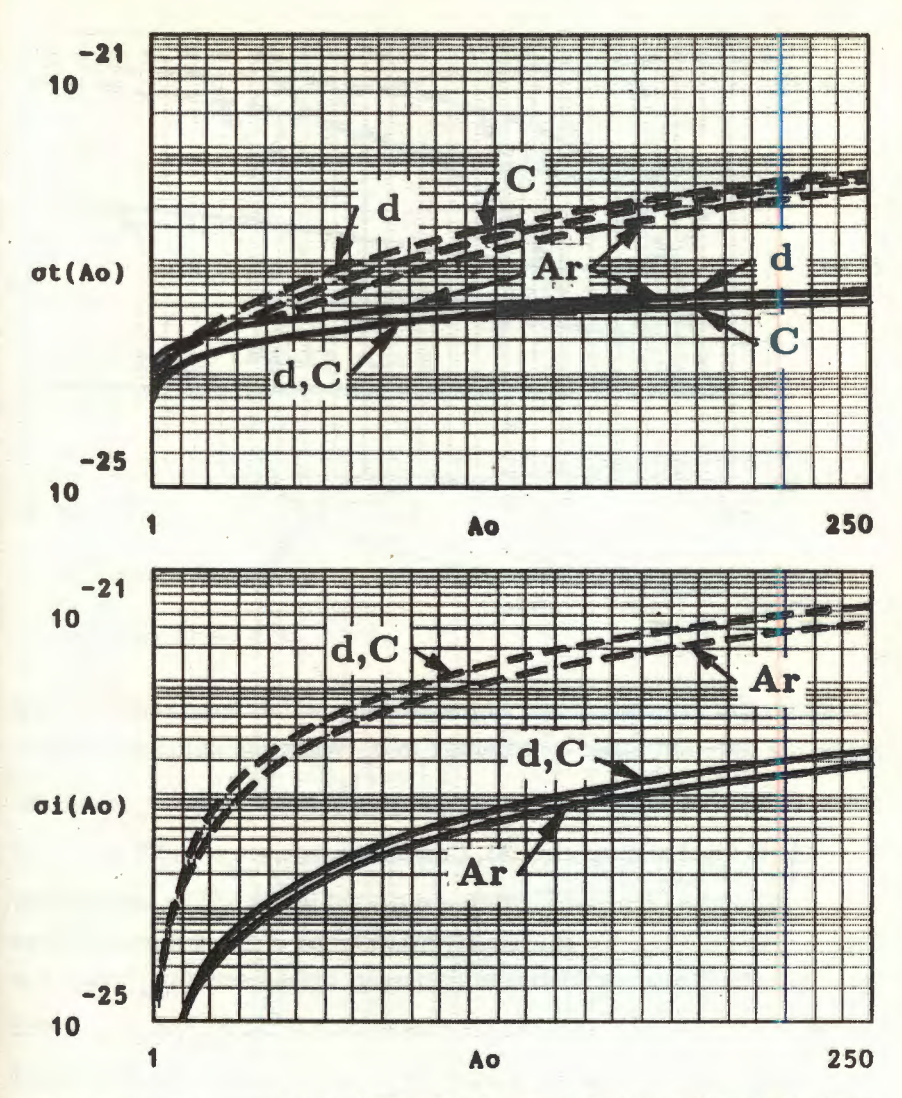


Fig. 3. The  $\sigma_i$  and  $\sigma_i$  cross sections of the loss of relativistic d, C and Ar nuclei at the Nuclotron vs target mass number  $A_0$  (-1 AGeV, -6 AGeV)

 $|\alpha_i| \approx 1.3$ ,  $D_i \approx 220$  cm,  $D_i' \approx 0.3$  at the target location). Effective cross section of the diffusion particle loss  $\sigma_i (i = x, z)$  and  $\sigma_t$  as a function of the target mass number  $A_0$  are shown in Fig.3. The values of the f()-function (see Fig.4) in eq.(7) show that for high energy heavy projectiles at the

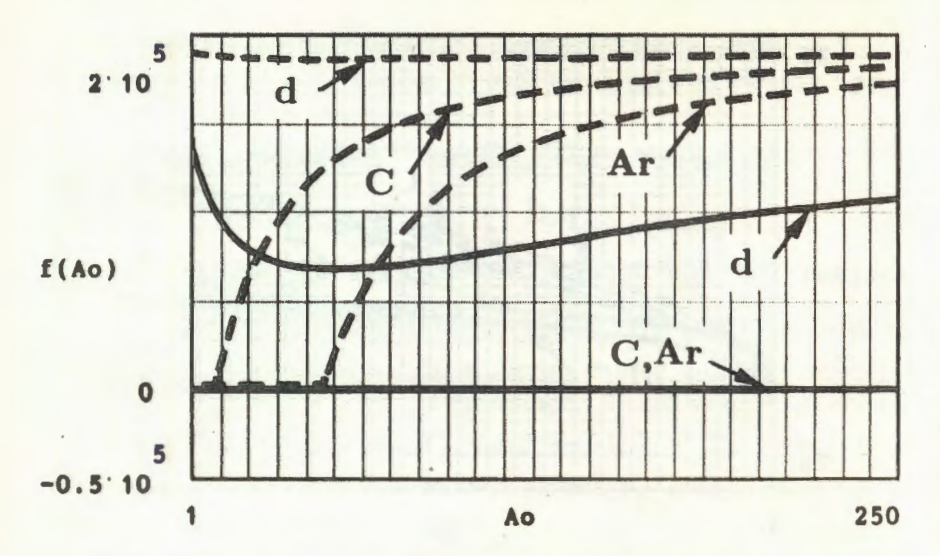


Fig. 4. The f()-function in  $\sigma_t$  vs target mass number  $A_0$  for different incident nuclei at the Nuclotron (-1 AGeV, ---6 AGeV)

Nuclotron (for example, C and Ar nuclei with  $\gamma=7.4$ ) large angle coulomb scattering does not make contribution to  $\sigma_t$ . When the initial beam emittances ( $\varepsilon_i^{(0)}$ ) are known, the corresponding values of T,  $\tau_i$  and  $T_b$  can be obtained from Fig.3 and eqs.(6), (8). Correlation between  $\tau_i$  and T is defined by the ai() and  $\overline{t}()$  functions, which are plotted in Fig.5. The presented in Figs.3,5 results show the substantial contribution of the diffusion process (related to small angle scattering in the target) to the losses ( $\sigma_{loss}$ ) of the low energy relativistic projectiles. As the energy increases the area of  $A_0$ , where this contribution is negligible, is grown by including larger mass numbers of the target. The maximum values of luminosities averaged over cycle time per one projectile at the first stage of Nuclotron run ( $T_c=10$  s) are plotted in Fig.6. As the internal target thickness  $t[g/cm^2]$  is known ( $t>t_c$ ) and using the presented in Fig.7 graphical functions of  $T_b \cdot t$ , the beam lifetime  $T_b$  [s] can be estimated. Assuming  $T_b=T_c$  in the value of  $T_b \cdot t$ -function the target thickness of  $t_c$  can be also obtained.

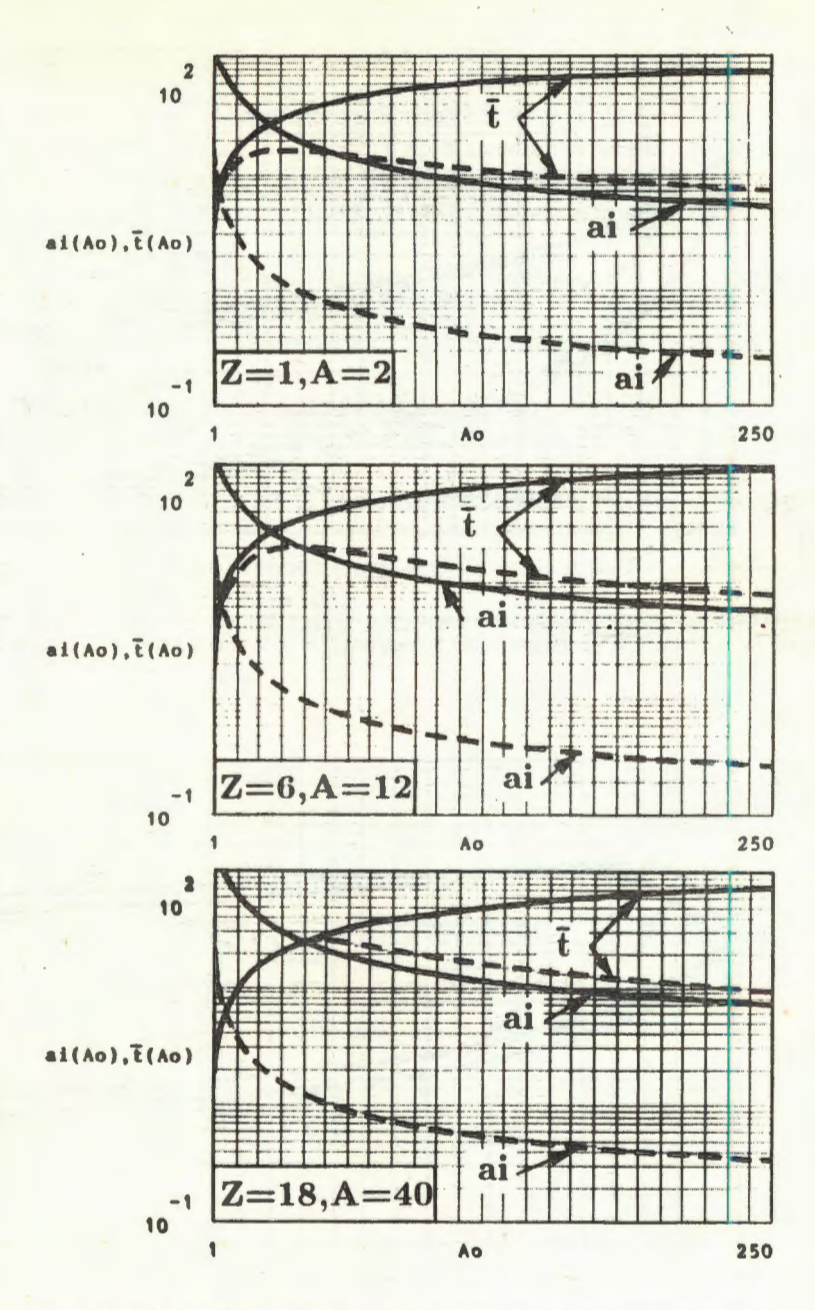


Fig. 5. The ai() and  $\overline{t}()$  functions vs target mass number  $A_0$  for different incident nuclei (- - 1 AGeV, --- 6 AGeV)

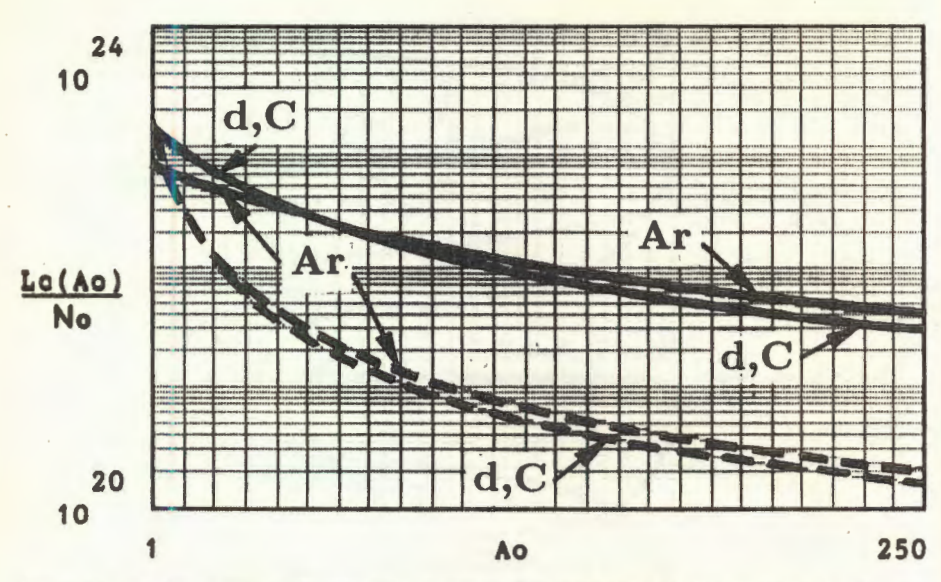


Fig. 6. The maximum values of luminosities averaged over cycle time per one projectile (d, C and Ar nulcei) for different internal targets at the Nuclotron ( $T_c = 10 \text{ s}, -1 \text{ AGeV}, -6 \text{ AGeV})$ 

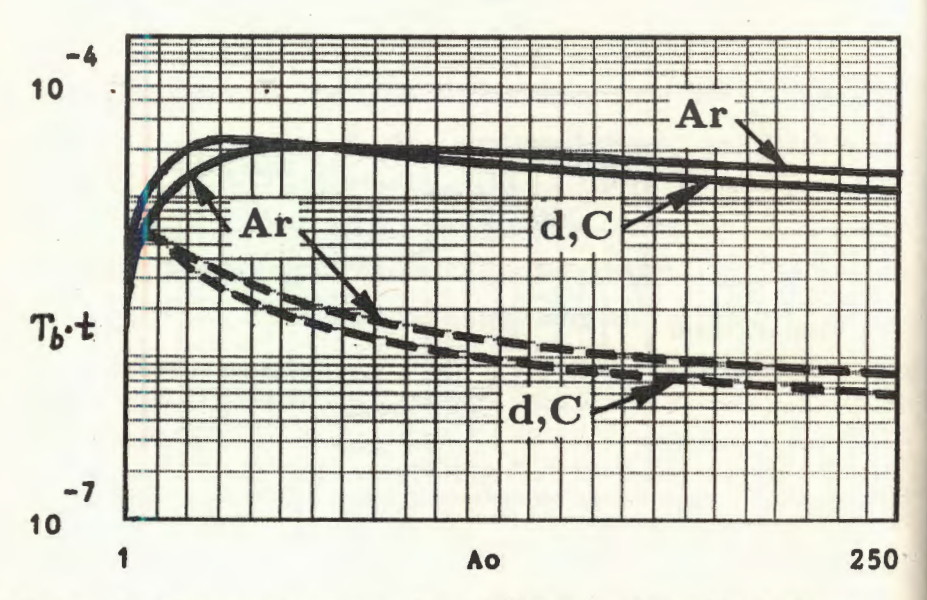


Fig. 7. The  $T_b \cdot t$ -functions vs target mass number  $A_0$  for different incident nuclei at the Nuclotron (-1 AGeV, ---6 AGeV)

## References

- 1. Baldin A.M. JINR Communication E1-92-487, Dubna, 1992.
- Baldin A.M. et al. JINR Rapid Communications, No.4[61]-93, Dubna, 1993, p.13.
- 3. Baldin A.M. et al. JINR Rapid Communications, No.2[65]-94, Dubna, 1994, p.26.
- 4. Hinterberger F., Mayer-Kuckuk T., Prasuhn D. Nucl. Instr. and Meth. A, 1989, vol.275, p.239.
- 5. Noda K., Noda A., Katayama I., Sakamoto N. Nucl. Instr. and Meth. A, 1991, vol.303, p.215.
- 6. Tschalar C. Nucl. Instr. and Meth. A, 1991, vol.308, p.471.
- 7. Hinterberger F., Prasuhn D. Nucl. Instr. and Meth. A, 1992, vol.321, p.453.
- 8. Artiomov A.S. JINR Rapid Communications, No.4[61]-93, Dubna, 1993, p.6.
- 9. Bruck H. Accelerateurs circulaires de particules, Paris: Presses Universitaires de France, 1966.
- Hinterberger F., Prasuhn D. Nucl. Instr. and Meth. A, 1989, vol.279, p.413.

### ACTIVELY SCREENED SC MAGNETS

### I.A.Shelaev

The concept of new actively screened SC magnets without a steel yoke for high energy accelerators is proposed, and their main features are discussed.

The investigation has been performed at the Laboratory of High Energies, JINR.

## Активно экранированные СП магниты

#### И.А.Шелаев

Предложена новая концепция активно экранированных СП магнитов без железного ярма для ускорителей высоких энергий и обсуждаются основные их свойства.

Работа выполнена в Лаборатории высоких энергий ОИЯИ.

### Introduction

In modern SC magnets the field strength and its quality are determined by a SC coil and its shape. Nevertheless, a cold steel yoke constitutes 80% and more of the magnet weight what significantly increases the magnet cost and time and cost of its cool-down and warm-up [1]. The steel yoke increases the magnet field only by 20—25%, and its main role is to shield stray fields. This task can be successfully resolved by an additional SC coil that only slightly increases the superconductor volume but drastically reduces the total magnet weight and its cost, and permits one to avoid such unpleasant features of the cold yoke as an additional energy losses due to steel magnetization in a pulse mode and nonlinearities with steel saturation at high fields.

We consider analytically the field of a shielded magnet and show how the volume of a superconductor should be increased to get a complete active shielding.

# 1. Ideal Magnet

Dipole and quadrupole fields required in high energy accelerators are produced by SC coils of two shapes [2]: overlapping ellipses and  $\cos \theta$  for a dipole field and crossed elipses or  $\cos 2\theta$  for a quadrupole one which provide

ideal fields. We consider overlapping ellipses, and it may be shown that  $\cos \theta$  coil is the limiting case of the latter.

The coil shape can be deduced using a straight cylindrical infinitely long conductor with a uniform current density j. If the conductor cross section is an ellipse with axes a and b (b < a), then its field H in complex form can be written as [3]

$$H = H_y + iH_x = \frac{0.4\pi j}{a+b} (bx - iay)$$
 (1)

inside the conductor and

$$H = \frac{0.4\pi jab}{z + \sqrt{z^2 - c^2}} \tag{2}$$

outside it. Here  $c^2 = a^2 - b^2$ , z = x + iy,  $i = \sqrt{-1}$  and the origin of the coordinate system coincides with the conductor center. The field is in G if the current density is expressed in  $A/cm^2$  and all linear dimensions in cm.

Two such conductors overlapped at a distance s between their centers and carrying the same current densities but of opposite signs produce a pure dipole field

$$H_y = \frac{0.4\pi j s b}{a+b}, \ H_x = 0$$
 (3)

inside the overlap region that is free of current. Two crossed similar conductors create a pure quadrupole field inside the aperture

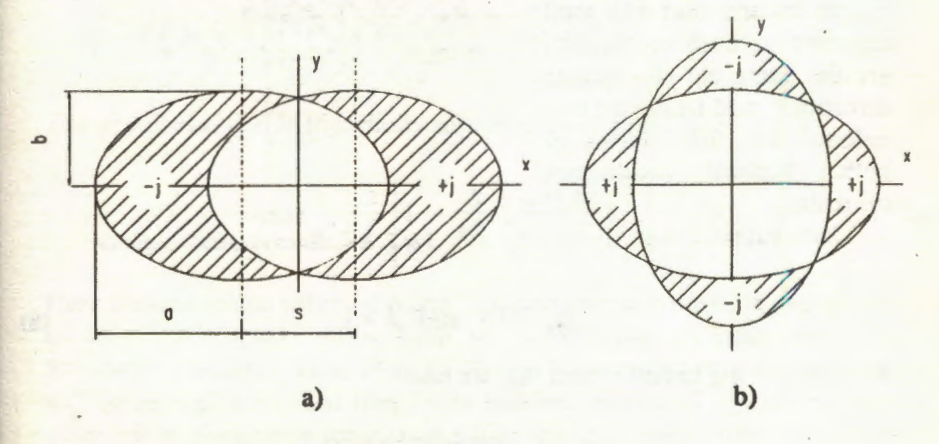


Fig.1. Coil cross sections of an ideal dipole a) and quadrupole b)

$$H_x = Gy, \ H_y = Gx, \ G = -0.4\pi j \frac{a-b}{a+b}.$$
 (4)

These two cases are shown in Fig.1. Dimensions of the ellipses have to be chosen such that to provide the required field strength or gradient at a given current density and to leave enough a current free space between them to place there a vacuum chamber for an accelerating beam. Evidently, the outside fields of the magnets are not equal to zero.

## 2. Screened Magnet

Let us consider now a similar elliptical conductor immersed into a bigger or screening one with axes  $a_s$ ,  $b_s$  and a current density  $j_s$  as shown in Fig.2.

The magnetic field outside this pair of conductors is equal to

$$H_{\text{out}} = 0.4\pi \left( \frac{jab}{z + \sqrt{z^2 - c^2}} + \frac{j_s a_s b_s}{z + \sqrt{z^2 - c_s^2}} \right). \tag{5}$$

The last equation shows that the outside field is zero if the following two conditions are fulfilled

$$jab = -j_s a_s b_s, \qquad (6)$$

$$c = c_s. \qquad (7)$$

$$c = c_{s}. (7)$$

Eq. (6) means that the total currents in both conductors are the same but of opposite directions, and from eq. (7) it follows that the focuses of both elliptical conductors coincide.

Now suppose that

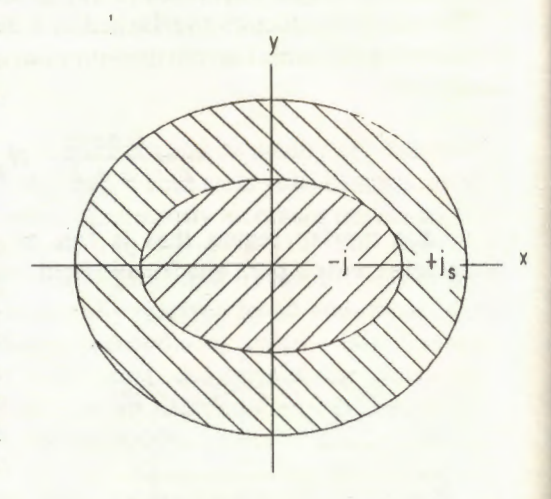


Fig. 2. A screened elliptical conductor

$$a_s = ka \text{ and } k > 1. \tag{8}$$

Then according to eq. (7) and (6), we find

$$b_s = \sqrt{b^2 + (k^2 - 1)a^2},\tag{9}$$

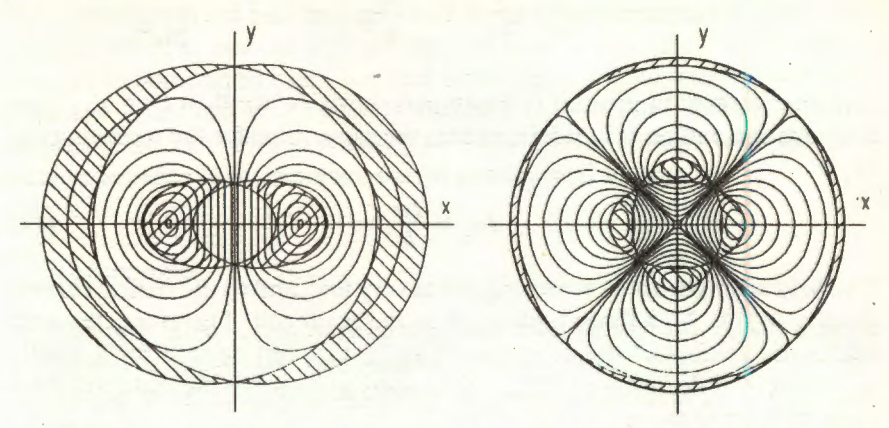


Fig. 3. Computer plot of the magnetic fields in a screened ideal dipole, on the left hand, and a quadrupole, on the right hand, for k = 2.5

$$j_s = -j \frac{b}{k\sqrt{b^2 + (k^2 - 1)a^2}} \approx -\frac{j}{k^2}.$$
 (10)

The last approximation is valid if  $a \approx b$  and k >> 1. This pair of screened conductors is used lower to construct ideal magnets as one eliptical conductor was used above.

If we now take another pair of similar conductors with as opposite currents as before and overlap (or cross) them, we shall get an ideal dipole (quadrupole) magnet without stray fields (Fig.3). Then the dipole field of the screened magnet is equal to

$$H_{ys} = -\frac{0.4\pi jbs}{a+b} \left[ 1 - \frac{a+b}{k(ka+b_s)} \right] = H_y(1-h), \ H_{xs} = 0.$$
 (11)

The gradient G inside the wholly screened quadrupole lens equals

$$G_{s} = -0.4\pi i \frac{a-b}{a+b} \left[ 1 - \frac{b}{kb_{s}} \left( \frac{a+b}{a_{s}+b_{s}} \right)^{2} \right] = G(1-g).$$
 (12)

Here dimensionless values of h and g show how much the field and gradient of screened magnets differ from the same value of unscreened coils. Evidently, a minimal value of k is 1 + s/a. If we choose larger k, then there will be enough a current free space between screening conductors and a main coil to place there force collars that constrain coil motion to negligible levels. The area S of the main dipole coil is equal to

$$S = 2ab \left( \arcsin \frac{s}{2a} + \frac{s}{2a} \sqrt{1 - \frac{s^2}{4a^2}} \right) \approx 2bs \left( 1 - \frac{s^2}{24a^2} \right).$$
 (13)

The total current in this coil or its ampere-turns Iw are then Iw = jS. From this equation and eq. (10) it follows that the same value for the screening coil  $Iw_c$  is

$$Iw_s \approx \frac{Iw}{k}$$
. (14)

The field strength at the screening coil is very low, and so the critical current density in it is 3-5 times higher the in the main coil. Therefore, the total additional volume of the superconductor in this coil needed for a wholly screening is of the order of 10% of the superconductor in the main coil if k is equal to 2.5 and more.

A SC volume needed to screen a quadrupole lens is even lower. The cross section area  $S_m$  of its main coil equals

$$S_m = 2ab \left( \arccos \sqrt{\frac{1 - e^2}{2 - e^2}} - \frac{\pi}{4} \right) \approx \frac{c^2}{2} \sqrt{1 - e^2},$$
 (15)

where  $e = ca^{-1}$  is the coil eccentricity. The area  $S_s$  of the screening coil is

$$S_s \approx \frac{c^2}{2} \sqrt{1 - \frac{e^2}{k^2}}$$
 (16)

or almost the same as the main coil area. Therefore, eq.(14) in the case of a quadrupole lens takes the form

$$Iw_{s} \approx -\frac{Iw}{k^{2}}. (17)$$

It reflects the fact that a field outside a dipole drops with a distance r as  $r^{-2}$  and a quadrupole  $r^{-3}$ . So the additional SC volume for screening a quadrupole coil is lower than in the case of a dipole.

## Conclusion

As is shown above, SC magnets without stray fields can be constructed at least in the two-dimensional case. The total additional volume of the superconductor in actively screened dipole magnets is 30—35% higher than in magnets with iron shielding but their weight 5—8 times lower.

Stray fields at the magnet ends need three-dimensional computer calculations. It is evident a priori that the screening will not be so wholly there as in considered case, but end stray fields will be much lower, and these low fields can be effectively shielded by soft steel walls of a warm vacuum vessel of a LHe cryostat. The walls are far enough from SC coils because between them there are one or two thermal screens.

## References

- Fisk H.E. Superconducting Magnets. Proc. of XIII Int. Conf. on High Energy Accelerators, Novosibirsk, «Nauka», 1987, 2, 15.
- Wilson M.N. Superconducting Magnets, Clarendon Press, Oxford, 1983, 29.
- Beth R.A. An Integral Formula for Two-Dimensional Fields, J. Appl. Phys., 1967, v.38, 12, pp.4689—4692.

# USING OF POLARIZED TARGET IN BACKWARD ELASTIC dp SCATTERING\*

I.M.Sitnik, V.P.Ladygin, M.P.Rekalo<sup>1</sup>

Effects due to the polarization of both colliding particles have been analysed in terms of four independent amplitudes which, in the general case, define the spin structure of the dp backward elastic scattering amplitude. It is shown, that spin correlation due to the transverse polarization of colliding particles has high sensitivity with respect to presumably existing P-wave in the deuteron. The experiments, needed to be performed for complete reconstruction of four independent amplitudes are discussed.

The investigation has been performed at the Laboratory of High Energies, JINR.

Использование поляризованной мищени в *dp* упругом рассеянии назад

# И.М.Ситник, В.П.Ладыгин, М.П.Рекало<sup>1</sup>

В терминах четырех независимых амплитуд, определяющих в общем случае спиновую структуру амплитуды упругого dp рассеяния назад, рассмотрены поляризационные эффекты, возникающие в случае, когда обе сталкивающиеся частицы поляризованы. Показано, что спиновая корреляция, связанная с поперечной поляризацией сталкивающихся частиц, обладает высокой чувствительностью по отношению к возможному существованию P-волны в дейтроне. Обсуждаются возможные эксперименты, необходимые для полного восстановления четырех независимых амплитуд.

Работа выполнена в Лаборатории высоких энергий ОИЯИ.

# 1. Introduction

Studying of the short-range behaviour of the deuteron wave function (DWF) allows us:

to understand the role of such non-nucleonic degrees of freedom as quark or delta configurations;

to clarify the transition regime from pion-nucleon mode to possible manifistation of the non-nucleonic degrees of freedom;

<sup>\*</sup>Report at Workshop on the Perspectives of Relativity Nuclear Physics, June 1994, Varna, Bulgaria

<sup>&</sup>lt;sup>1</sup>KhPTI, Kharkov, Ukraine

to check the different approaches of description of the relativistic bound states.

A direct reconstruction of the DWF from the measured quantities in the framework of the Impulse Approximation (IA) is possible in two types of reactions. They are deuteron electrodisintegration [1]  $ed \rightarrow e + np$ , and also A(d,p)X and p(d,p)d reactions [2,3].

The momentum distributions of fragments extracted from the data of the above experiments with electromagnetic and nuclear probes demonstrate, on the one hand, a substantial discrepancy with the predictions using standard DWF in the IA and, on the other hand, a good agreement with one another [4,5], which gives serious motivations to search for the explanation of the observed effects not only in deviation from the IA but also in nonadequate standard DWF. Even at the IA level the following questions arise:

the number of independent components of the DWF (two in nonrelativistic theory including S- and D-waves or four in relativistic theory including S-, P- and D-waves [6], or six in the spurion models [7]);

what is the argument of the DWF and furthermore the number of them (one as in standard models or two as in spurion approaches);

possible non-nucleonic degrees of freedom  $(NN^*, \Delta\Delta)$  of the deuteron.

To determine the behaviour of different components of the DWF, one needs to study polarization observables of the above reactions, because they are more sensitive to smaller terms than cross section. At the present time such data exist or are in progress only for nuclear probe reactions. Apart from cross sections, such observables as the tensor analyzing power  $T_{20}$  and the polarization transfer coefficient from the deuteron to the proton  $\kappa_t$  have been investigated for the reactions  $A(\mathbf{d},p)X$  and  $p(\mathbf{d},p)d$ . Analysis of each of these reactions points out [8,9,10] no configuration consisting only of S-and D-waves are compatible with the data within the framework of the IA.

The existing set of data is insufficient to separate the deuteron structure from the reaction mechanism. So, measurements of new polarization observables are needed. They can be obtained using a polarized proton target for backward dp elastic scattering (but not for the reaction A(d,p)X). The measurements of these observables are being planned now at Dubna.

# 2. Amplitude of the $d+p \rightarrow p+d$ ( $\theta=180$ ) Process and General Analysis of the Polarization Effects

Backward dp elastic scattering due to P-invariance and total helicity conservation can be described by only four independent complex amplitudes for the following transition  $\lambda_d$ ,  $\lambda_p \rightarrow \lambda_d'$ ,  $\lambda_p'$ ,

$$F_{0+\to 0+} = g_2(s),$$

$$F_{++\to ++} = g_1(s) + g_4(s),$$

$$F_{-+\to -+} = g_1(s) - g_4(s),$$

$$F_{0+\to +-} = -\sqrt{2} g_3(s),$$
(1)

where  $g_1 - g_4$  are so named scalar amplitudes. Of course, all polarization effects can be described in terms of the scalar or helicity amplitudes.

In case of unpolarized target the differential cross section  $\frac{d\sigma^{(T0)}}{d\Omega}$  depends only on the tensor polarization  $P_{NN}$  of initial deuterons:

$$\begin{split} \frac{d\sigma^{(T0)}}{d\Omega} &= \frac{d\sigma^{(00)}}{d\Omega} \left( 1 + \frac{1}{2} P_{NN} C_{0,NN,0,0} \right), \\ N^{-1} \frac{d\sigma^{(00)}}{d\Omega} &= 2 |g_1(s)|^2 + |g_2(s)|^2 + 2 |g_4(s)|^2, \\ C_{0,NN,0,0} N^{-1} \frac{d\sigma^{(00)}}{d\Omega} &= -|g_1(s)|^2 + |g_3(s)|^2 - |g_4(s)|^2, \end{split} \tag{2}$$

where  $\frac{d\sigma^{(00)}}{d\Omega}$  is the differential cross section for unpolarized initial particles, and  $C_{0,NN,0,0}$  is the analyzing power due to tensor polarization of the initial deuteron. (Here we are following notations used in ref. [11].)

The expressions for the normal  $(C_{0,N,N,0})$  and longitudinal  $(C_{0,L,L,0})$  polarization transfer coefficients from the vector-polarized deuteron to the secondary proton are

$$C_{0,N,N,0}N^{-1} \frac{d\sigma^{(T0)}}{d\Omega} = 2 \cdot \text{Re} \left[ g_3(s) \cdot \left[ g_1(s) + g_2(s) + g_4(s) \right]^* \right],$$

$$C_{0,L,L,0}N^{-1} \frac{d\sigma^{(T0)}}{d\Omega} = 2 \cdot \left\{ \left| g_3(s) \right|^2 + 2\text{Re} \left[ g_1(s) \cdot g_4(s)^* \right] \right\}. \tag{3}$$

Discussed above polarization observables  $T_{20}$  and  $\kappa_t$  are connected with used in (2) and (3) as

$$T_{20} = -\sqrt{2} C_{0,NN,0,0}$$

$$\kappa_t = \frac{3}{2} C_{0,N,N,0} \,. \tag{4}$$

If the proton target is polarized, the differential cross section depends on mutual spin orientation of initial protons and deuterons

$$\frac{d\sigma}{d\Omega} = \frac{d\sigma^{(T0)}}{d\Omega} \left[ 1 + \frac{3}{2} C_{N,N,0,0} (SP - (nS)(nP) + \frac{3}{2} C_{L,L,0,0} (nS)(nP) \right].$$
 (5)

From (5) one can see that the term  $C_{N,N,0,0}(C_{L,L,0,0})$  is responsible for the asymmetry effect when spin orientations of both participants of the reaction are normal (longitudinal) to the direction of the initial deuteron 3-momentum.

In terms of scalar amplitudes the expressions for spin correlation parameters  $C_{N,N,0,0}$  and  $C_{L,L,0,0}$  are following:

$$C_{N,N,0,0}N^{-1}\frac{d\sigma^{(T0)}}{d\Omega} = -2 \cdot \text{Re} \left[ g_3(s) \cdot \left[ -g_1(s) - g_2(s) + g_4(s) \right]^* \right],$$

$$C_{L,L,0,0}N^{-1}\frac{d\sigma^{(T0)}}{d\Omega} = -2 \cdot \left\{ \left[ g_3(s) \right]^2 - 2\text{Re} \left[ g_1(s) \cdot g_4(s)^* \right] \right\}. \tag{6}$$

In contrast to the differential cross section and  $C_{0,NN,0,0}$ , expressions for spin correlations and polarization transfer coefficients contain the interference contributions  $\text{Re}(g_i \cdot g_k^*)$ , hence, these observables are particularly sensitive to the smallest terms.

For realization of the complete experiment program it is necessary to obtain data for the polarization observables containing the  $\text{Im}(g_i \cdot g_k^*)$  contributions. Needed combinations appear only for triple correlations of vector polarizations:

$$S_1 \times S_2 \cdot S_3$$
,  $nS_1 \cdot nS_2 \times S_3$  (7)

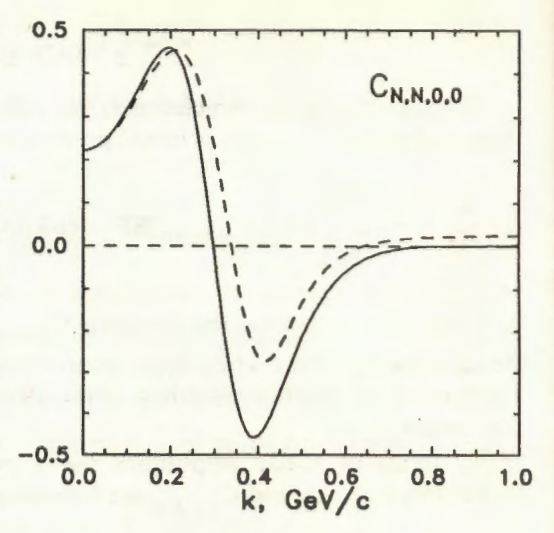
and so on, where  $S_i$  is the polarization vector of an *i*-particle. We would like to stress that polarization transfer measurements, in case all three particles have various combinations of parallel or antiparallel spins, do not provide needed information.

Within the IA (one nucleon exchange mechanism) with standard DWF only two amplitudes (real in this case) define all characteristics of the discussed reaction.

Spin correlation  $C_{N,N,0,0}$  calculated for standard DWF [13] (solid line) and for DWF with additional P-wave components [6] (dashed line)

The various models of the deuteron with additional P-wave [6,12] components are compatible with the case, when the process is described by four independent (but real) amplitudes.

Calculations of  $C_{N,N,0,0}$  performed for one of standard DWF [13] within the IA (Figure), demonstrate rather the scale of the effect than really



expected behaviour, because, as it was mentioned above, this approach is not compatible with the results of experiments. One can see high sensitivity of  $C_{N,N,0,0}$  to P-wave contribution.

More detailed consideration of all these question is given in [14].

# 3. Conclusions

Measurement of the spin correlation parameter  $C_{N,N,0,0}$  is one of the most realizable polarization experiments for the  $d+p \Rightarrow p+d$  to date. These data (in addition to measured cross section [3], tensor analyzing power  $T_{20}[8,10]$  and polarization transfer coefficient  $\kappa_t$  [8]) could provide us to determine  $g_1-g_4$  amplitudes in the case they are real. Within IA it is possible to estimate a possible P-wave component in the deuteron.

To determine the imaginary parts of  $g_1 - g_4$  amplitudes one needs to perform complicated transfer polarization experiments in case of both polarized initial particles. But if all three particles have various combinations of parallel or antiparallel spins, the measurements of these triple-order observables do not provide us information about imaginary parts of  $g_1 - g_4$  amplitudes.

The authors would like to express their gratitude to A.M.Baldin, J.Durand, B.A.Khachaturov, N.B.Ladygina, F.Lehar, A.de Lesquen,

N.M.Piskunov, C.F.Perdrisat, V.Punjabi for useful discussions and stimulating interest in the present work.

## References

- 1. Bosted P. et al. Phys. Rev. Lett., 1982, 49, p.1380.
- Ableev V.G. et al. Nucl. Phys., 1983, A393, p.491;
   Ableev V.G. et al. JINR Rapid Comm. 1 [52], Dubna, 1992, p.10.
- 3. Berthet P. et al. J. Phys. G.: Nucl. Phys., 1982, 8, p.L111.
- 4. Ableev V.G. et al. Pis'ma JETF, 1983, 37, p.196.
- 5. Kobushkin A.P. J. Phys. G.: Nucl. Phys., 1986, 12, p.487.
- 6. Buck W.W., Gross F. Phys. Rev., 1979, D20, p.2361.
- 7. Karmanov V.A. EChAYa, 1988, 19, p.525.
- 8. Punjabi V. et al. In: Proceedings of 14-th Int. IUPAP Conf. on Few Body Problems in Physics, Willjamsburg, USA, May 1994, p.161.
- Kuehn B., Perdrisat C.F., Strokovsky E.A. Dubna Deuteron-93 Symp. (to be published).
- 10. Azhgirey L.S. et al. JINR Preprint E1-94-156, Dubna, 1994.
- 11. Ghazikhanian V. et al. Phys. Rev., 1991, C43, p.1532.
- 12. Glozman L.Ya., Neudatchin V.G., Obukhovsky I.T. Phys. Rev., 1993, C48, p.389.
- 13. Lacombe M. et al. Phys. Lett., 1981, 101, p.139.
- 14. Sitnik I.M., Ladygin V.P., Rekalo M.P. JINR Preprint E1-94-23, Dubna, 1994 (to be published in Sov. Journ. Nucl. Phys., 1994, No.12).

# APPLICATION OF TRANSPUTERS IN THE DATA ACQUISITION SYSTEM OF THE INESS-ALPHA SPECTROMETER\*

## E.V.Chernykh

The paper describes the application of transputers in the DAQ system of the INESS-ALPHA spectrometer used in investigations of polarization phenomena in a few-rection systems under relativistic energies. The system has multiprocessor structure according to a scheme: main IBM PC plus add-on transputer-based boards. The system comprises three sub-systems interconnected by message transmission. The HW of the system and characteristic properties of application of transputers are under consideration, some promises of 'transputer-like' microprocessors using in DAQ systems are mentioned. The SW for the system is described in [1].

The investigation has been performed at the Laboratory of High Energies, JINR.

# Применение транспьютеров в системе сбора данных спектрометра ИНЕСС-АЛЬФА

# Е.В. Черных

В работе описано применение транспьютеров в системе сбора данных спектрометра ИНЕСС-АЛЬФА. используемого исследованиях явлений малонуклонных системах поляризационных B релятивистских энергиях. Система имеет многопроцессорную структуру в соответствии со схемой: основная ЭВМ ІВМ РС плюс дополнительные транспьютерные платы. Система состоит из трех подсистем, связанных механизмом передачи сообщений. Рассмотрены аппаратное обеспечение системы и особенности применения транспьютеров, кратко упомянуты перспективы применения транспьютероподобных микропроцессоров в системах сбора данных. Программное обеспечение системы описано в работе [1].

Работа выполнена в Лаборатории высоких энергий ОИЯИ.

## 1. Introduction

In 1993 according to the research program of investigations of polarization phenomena in a few nucleon systems under relativistic energies experiments were begun using polarized deuteron beams of JINR

<sup>\*</sup>The paper was presented at SPHERE-ALPHA workshop, June 1994, Varna, Bulgaria

synchrophasotron and INESS-ALPHA set-up [2,3]. The two-arm magnet spectrometer INESS-ALPHA incorporates 2000 channels of coordinate and spectrometric information, front-end electronics is located in seven crates of a standard CAMAC parallel branch highway [4,5]. The existed DAQ system of the set-up has not met new requirements, therefore a new DAQ system has been developed. As this was done the front-end electronics has not been changed. It was required, among other things, to enlarge a number of accepted events, to provide recording of the extracted beam data and accelerator parameters from remote control system of the accelerator and perform analysis of the experimental data during run. Under conditions of very limited expenditure some basic principles of the DAQ system development were formulated: low initial expenditure, use of standard means, possibility of modular extension.

# 2. The Application of Transputers

If the DAQ system for the spectrometer had been implemented, using single computer the unexeptable expenditure and complicated system would have been needed. So the system has multiprocessor structure: main computer plus add-on boards installed in its I/O slot. To provide an acceptable expenditure/performance ratio the IBM PC as the main computer and transputer-based add-on boards were selected. The advantages of the PC are well known: accessibility, low cost, it is provided with many HW and SW add-on's and good service.

Transputers are intended to serve as building blocks for real-time parallel systems [6]. Transputer (processor) compared to common microprocessor additionally contains in silicon internal RAM, timers, links and OS kernel. Members of the transputer product family are interconnected by their links — high speed serial duplex lines. There are processors, link adapters and programmable links commutators in the transputer family. The link adapter converts between serial link and parallel bus, link commutator provides a full crossbar switch between 32 link inputs and 32 link outputs.

To build a microcomputer using transputers one needs less additional ICs. A transputer gives to the system the following features:

- enlargement of data processing power;
- highly reliable interconnections;
- first-rate performance to stand-alone devices.

In accordance with the requirements during preparation and running the experiment the DAQ system comprises the following subsystems (Figure):

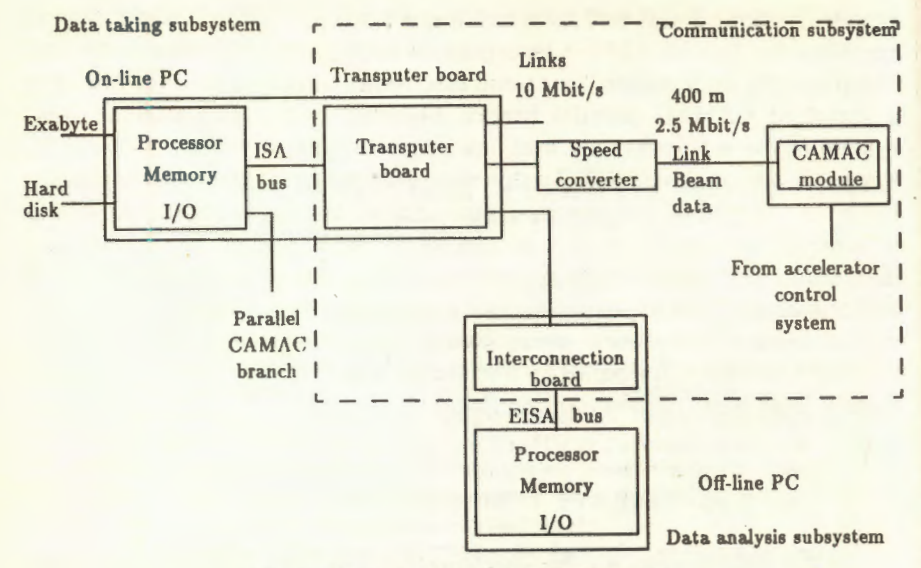


Figure. Structure diagram of the DAQ system

- data taking and on-line processing (consists of the on-line PC and transputer board);
- communication (transputer and interconnection boards, speed converter);
  - data analysis during run (off-line PC).

The on-line PC reads data from the CAMAC branch, preprocesses them, builds the file and writes it to the hard disk. Between the accelerator cycles the data from the disk buffer are written to Exabyte tape and transmitted to the off-line PC for data analysis during the run.

The transputer board in the on-line PC uses transputer links to accept the data transferred from the accelerator control system and to synchronize processes in the subsystems. The transputer board incorporates processor T414, 1 Mbyte RAM and the interface of ISA-bus program channel implemented using the first transputer link and Link Adapter C011 [7]. Via the second transputer link the data describing the extracted beam and accelerator tuning from the accelerator control computer spaced at 400 meters are accepted. This data are transmitted by CAMAC module based on Link Adapter. The speed of a type transmission is 2.5 Mbit/sec. Thus the Link Adapter is used beyond the specification but no errors during the data transmission were detected. A speed converter implemented using two Link Adapters converts the bit speed after the receiver up to a standard for the transputer family value 10 Mbit/sec and transmits the byte to the transputer

board. The transputer transmits the data in the data file of events using interrupts in the on-line PC. The third link of the transputer is used to transmit data to the off-line PC via an add-on board with C011 placed in an I/O slot of the PC. For communication between the subsystems the message transmission mechanism is used.

During three runs in 1993—94 about 1.5 gigabyte of experimental data were stored to Exabyte tape. Different PCs were used in the course of the experiments: PC/386 ISA, 486 EISA, 486 ISA.

# 3. Promising Transputer-Like Microprocessors for DAQ systems

An intrinsic parallelism which has data acquisition and triggering usage and specific features of transputers made possible application of them in these systems [8]. A DAQ system for the general-purpose detector ZEUS at the HERA collider comprises 640 transputers [9].

New generation of Inmos transputer family offers increased computer power and higher speed links [10]. New generation components for HEP applications based on this ICs were developed [11]. A number of large experiments in HEP being planned (for example STAR) and those which have used transputers yet (for example ZEUS) consider them among other microprocessors as a promising means to use in the DAQ system. The most interesting for DAQ systems in HEP is the Inmos message routing chip C104.

Transputer had influence on microprocessor development. Large firms designed and produce transputer-like microprocessors, which are intended for multiprocessor systems development and furnished with communication channels (Texas Instruments TMS320C40, Motorola DSP96002, Analog Devices ADSP-21060). Quite a lot of new designs for trigger systems use C40, Motorola DSP96002 is also used. The new ADSP-21060 shows promise for the applications under consideration. The emergency of the Power PC with features well like a workstation but the cost much less gives an opportunity to develop DAQ systems having good performance/cost ratio on the base of the PC in conjunction with these new microprocessors.

# 4. Conclusions

The application of transputers in conjuction with IBM PC provided for the DAQ system a reliable means for a communication and a high-speed data processing power. The system reads up to 500 events per cycle (event length is about 300 bytes), that gives the speed of data taking 150 Kbyte/sec. The system structure makes it possible autonomous debugging of the subsystems, data analysis during the run and modular extension of the system. In three runs 1.5 gigabyte of experimental data have been stored to Exabyte tape. The results of some experiments have been published [12,13]. New generation transputers and transputer-like microprocessors integrally with Power PC hold great promise for new DAQ systems of new experiments.

# 5. Acknowledgments

The DAQ system of the INESS-ALPHA spectrometer was developed in collaboration with S.A.Zaporozhets. I would like to acknowledge the continuous support of A.D.Kovalenko and N.M.Piskunov and I am grateful to colleagues of ALPHA collaboration and V.I.Prikhodko and V.N.Polyakov of JINR LNP for their help.

### References

- Zaporozhets S.A. Report presented at SPHERE-ALPHA Workshop, Varna, Bulgaria, June, 1994.
- 2. Piskunov N.M. ibid.
- 3. Ladygin V.P. ibid.
- 4. Ableev V.G. et al. PTE, 1978, №2, p.63 (in Russian).
- 5. Ableev V.G. et al. PTE, 1983, №1, p.33 (in Russian).
- 6. SGS-Thompson, Inmos Transputer Data Book, Second Edition, 1989.
- Leich A. et al. In: Proceed. XIII JINR Intern. Sympos. on Nuclear Electronics, JINR, D13-88-938, Dubna, 1988, p.54.
- 8. Dobinson R.W. et al. Partcile World, 1991, vol.2, №2, p.39.
- 9. Kovalski H. In: Proceed. Computing in HEP'92, CERN 92-07, p.33.
- Sheperd R. et al. In: 1991 CERN School of Computing, CERN 92-02, 14 May 1992, pp. 295, 309, 323.
- 11. Martin B. et al. In: Proceed. 8th Conf. on Real-Time Computer Applications, Vancouver, Canada, June 8—11, 1993 TRI-93-1, p.74.
- Azhgirey L.S. et al. In: Proceed. Intern. IUPAP Conf. on Few Body Problems in Physics, May 26-31, 1994, Williamsburg, USA, p.18 and JINR Preprint E1-94-155, Dubna, 1994.
- Azhgirey L.S. et al. ibid, p.22 and JINR Preprint E1-94-156, Dubna, 1994.

# NARROW DIBARYON RESONANCES WITH ISOTOPIC SPIN I = 2

Yu.A.Troyan, V.N.Pechenov, E.B.Plekhanov, S.G.Arakelian, A.Yu.Troyan, V.I.Moroz, A.P.Ierusalimov, A.P.Stelmakh

Narrow enhancements were observed in the effective mass spectrum of  $pp\pi^+$ -combinations at  $(2511\pm5)$ ,  $(2607\pm2)$  and  $(2716\pm4)$  MeV/c<sup>2</sup> in the reaction  $np \rightarrow pp\pi^+\pi^-\pi^-$  at an incident momentum of  $P_n = 5.2\pm0.16$  GeV/c, studied in the 1m bubble chamber, LHE, JINR. The total experimental widths of the resonances are equal to 46, 27 and 36 MeV/c<sup>2</sup> and are completely determined by the resolution of the apparatus. The enhancements above background are 4.0; 6,8 and 3.4 standard errors. The most probable value of the spin for the resonance with a mass of 2607 MeV/c<sup>2</sup> was found to be  $J \ge 2$ . The resonance with such a mass decays with a probability of 48% via the mode  $\Rightarrow \Delta_{33}p$ , with a probability of 14% via  $\Rightarrow (BB)_{2090}^{++}$  and 38% via other modes. Here  $(BB)_{2090}^{++}$  is a dibaryon in a 2-proton system with a mass around 2090 MeV/c<sup>2</sup>.

The investigation has been performed at the Laboratory of High Energies and at the Laboratory of Computing Techniques and Automation, JINR.

Узкие дибарионные резонансы с изотопическим спином I = 2

# Ю.А.Троян и др.

В реакции  $np opp pp^+\pi^-\pi^-$  при импульсе первичных нейтронов  $P_n = 5,2\pm0,16$  ГэВ/с на материалах с 1-метровой водородной пузырьковой камеры ЛВЭ ОИЯИ обнаружены узкие особенности в спектре эффективных масс  $pp\pi^+$ -комбинаций при значениях (2511 $\pm$ 5), (2607 $\pm$ 2) и (2716 $\pm$ 4) МэВ/с². Полные экспериментальные ширины резонансов равны 46, 27 и 36 МэВ/с² и целиком определяются аппаратурным разрешением. Превышение над фоном составляет 4,0; 6,8 и 3,4 стандартных отклонения соответственно. Наиболее вероятное значение спина резонанса с массой 2607 МэВ/с² оказалось равным  $J \ge 2$ . Этот резонанс распадается с вероятностью около 48% по каналу  $\rightarrow$   $\Delta_{33}P$ , с вероятностью около 14% по каналу  $\rightarrow$  (ВВ) $^{++}_{2090}\pi^+$  и с вероятностью около 38% по другим каналам. Здесь (ВВ) $^{++}_{2090}$  — дибарион в системе 2-х протонов с массой в районе 2090 МэВ/с².

Работа выполнена в Лаборатории высоких энергий и Лаборатории вычислительной техники и автоматизации ОИЯИ. The presented results were obtained by processing the films in an exposure of 1m hydrogen bubble chamber, LHE, JINR, to monochromatic neutrons ( $\Delta P_n/P_n \approx 3\%$ ) at a momentum of 5.20 GeV/c. The characteristics of the beam, methods of the selection of reaction channels, the reaction cross-sections, etc., were described earlier ([1], see refs.). The following reactions were identified from 5-prong stars:

$$np \to pp\pi^{+}\pi^{-}\pi^{-} \quad (10356 \text{ events}) \tag{1}$$

$$np \to pp\pi^{+}\pi^{-}\pi^{-}\pi^{0}$$
 (6357 events). (2)

Figure 1 shows the distribution of effective masses of  $pp\pi^+$ combinations: 1) — from reaction (2), 1) — from reaction (1), 3) — sum of

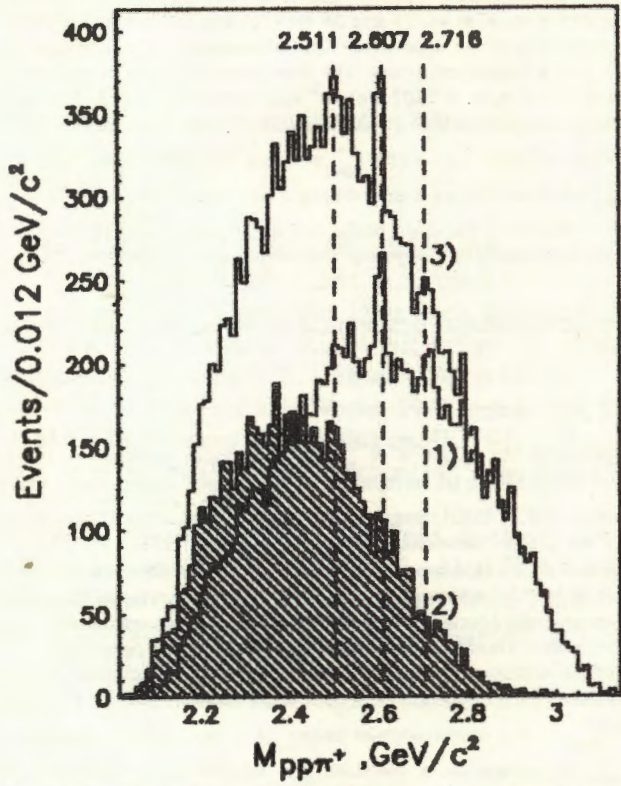


Fig.1. The effective mass distribution of  $pp\pi^+$ -combinations at  $P_n=5.2$  GeV/c: 1) — reaction  $np \rightarrow pp\pi^+\pi^-\pi^-$ ; 2) — reaction  $np \rightarrow pp\pi^+\pi^-\pi^-\pi^0$ ; 3) — sum of (1) and (2)

these reactions. One can easily note an enhancement near masses of 2500, 2600 and 2700 MeV/ $c^2$ , which repeats for all distributions.

The further analysis is concerned mainly with reaction (1).

Figure 2 shows the distribution of effective masses of  $pp\pi^+$ -combinationns from reaction (1). The distribution is approximated by an incoherent sum of the background curve taken in the form of a superposition of Legendre polynomials of up to the second power inclusive (coefficients of higher power polynomials are negligible), and by three Breit — Winger resonance curves. The background contributes up to 95.3%. The

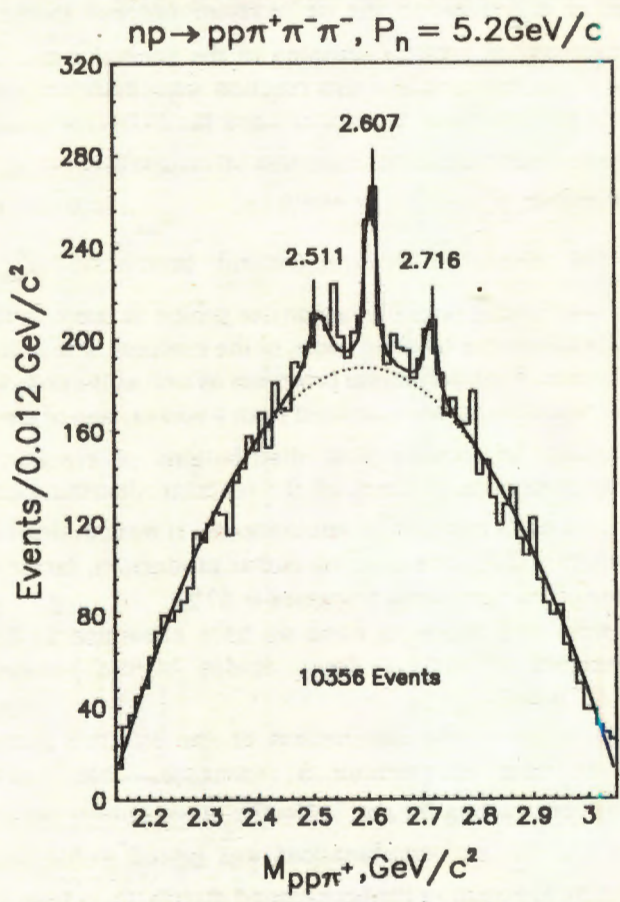


Fig. 2. The effective mass distribution of  $pp\pi^+$ -combinations from reaction (1) at  $P_n = 5.2$  GeV/c. The solid line — the approximation by the background curve and three Breit — Wigner curves; dotted line — the contribution of the background (Legendre polynomial of second power)

background describes the regions outside the resonances with  $\chi^2 = 0.8 \pm 0.18$ ,  $\sqrt{D} = 1.57 \pm 0.12$ , that is close to the pure statistical distribution with  $\chi^2 = 1.0$ ,  $\sqrt{D} = 1.41$ .

The central values of the masses of the observed resonances are equal to  $(2511\pm5)$ ,  $(2607\pm2)$ ,  $(2716\pm4)$  M<sub>3</sub>B/c<sup>2</sup>. The exceedings over the background are equal to 4.0, 6.8 and 3.4 standard deviations, respectively. More detailed data are presented in the final table.

The analysis showed the reaction (1) proceeded largely through a

production of  $\Delta_{33}$ -isobar in the  $p\pi^+$ -system and was characterized by a strong anisotropy of protons emission in the general c.m.s. For the subsequent analysis the events of this reaction were therefore simulated with and without production of  $\Delta_{33}$ -isobar using the FOWL program. Moreover, the periphericity of protons emission was taken into account by introducting the factor  $\exp B \mid y_{p_1}^* - y_{p_{\min}}^* \mid * \exp B \mid y_{p_2}^* - y_{p_{\max}}^* \mid$  into the phase spase,  $y_{p_1(p_2)}^*$  — the rapidity of the first (second) proton, and  $y_{\min(\max)}^*$  — the minimum (maximum) possible rapidity of proton in reaction (1) at present energy. All values were taken in c.m.s. of the reaction. The value of factor B, the contribution of the peripheral processes as well as the contribution of the  $\Delta_{22}$ -production channel were defined from a comparison of simulated event with a number of experimental distributions of reaction (1) (angle distribution of protons in c.m.s. of the reaction, distributions of effective masses of pp-,  $p\pi$ <sup>+</sup>- and  $pp\pi$ <sup>+</sup>-combinations). It was obtained that reaction (1) proceeded in 50% of events via isobar production; factor B = 3.3, the contribution of the peripheral processes ≈ 57%.

With simulated events at hand we have attempted to determine the relative weights of various decay modes of the resonance with a 2607 MeV/c<sup>2</sup> mass.

Figure 3a shows the distribution of the effective masses of  $p\pi^+$ -combinations from the mentioned resonance. This distribution was obtained by constructing the  $pp\pi^+$  effective masses under the condition that at least one of the  $p\pi^+$ -combinations was placed within the  $\Delta_{33}$ -isobar region, and by subtracting the background distributions from left and right sides of the band of 2607 MeV/c<sup>2</sup> resonance with the corresponding weights determined by the background contribution in the resonance band. The distribution is described by the curve composed by 70% due to resonance curve of  $\Delta_{33}$ -resonance and by 30%, due to phase space curve.

Figure 3b shows the effective mass distribution of two protons from mentioned resonance, obtained in the same way. The distribution is described by the curve with 40% due to the curve of pp-resonance with a mass around 2090 MeV/c² and 60%, due to the background curve caused by the sum of processes in reaction (1) (with — and without  $\Delta_{33}$ -production, and taking into account the periphericity of protons). The narrow pp-resonances with masses around 2090 MeV/c² were observed in a number of experiments [2]

In consequence, the following values were obtained for the relative contributions of various decay modes of the resonance in  $pp\pi^+$ -system at the 2607 MeV/ $c^2$  mass:

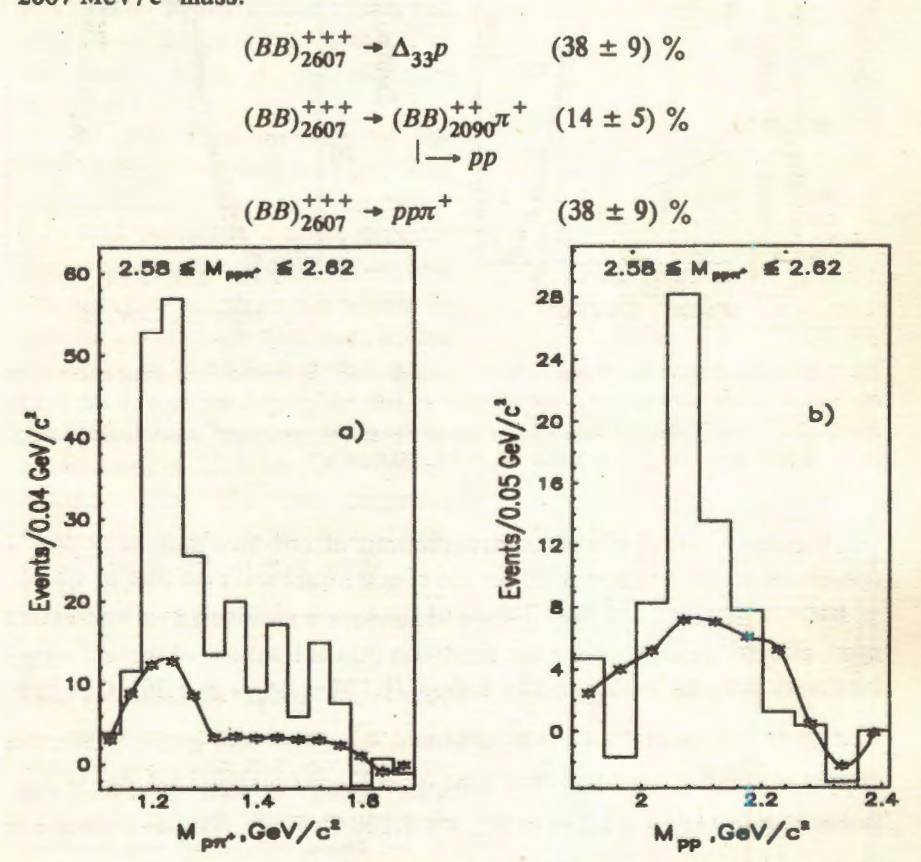


Fig. 3. a) — The effective mass distribution of  $p\pi^+$ -combinations for  $pp\pi^+$ -resonance with 2607 MeV/c<sup>2</sup> mass. Crosses — the contribution of the background due to the periphericity of phase space. b) — The effective mass distributions of pp-combinations for  $pp\pi^+$ -resonance with 2607 MeV/c<sup>2</sup> mass. Crosses — the contribution of the background due to processes of  $\Delta_{33}$ -production and periphericity of phase space

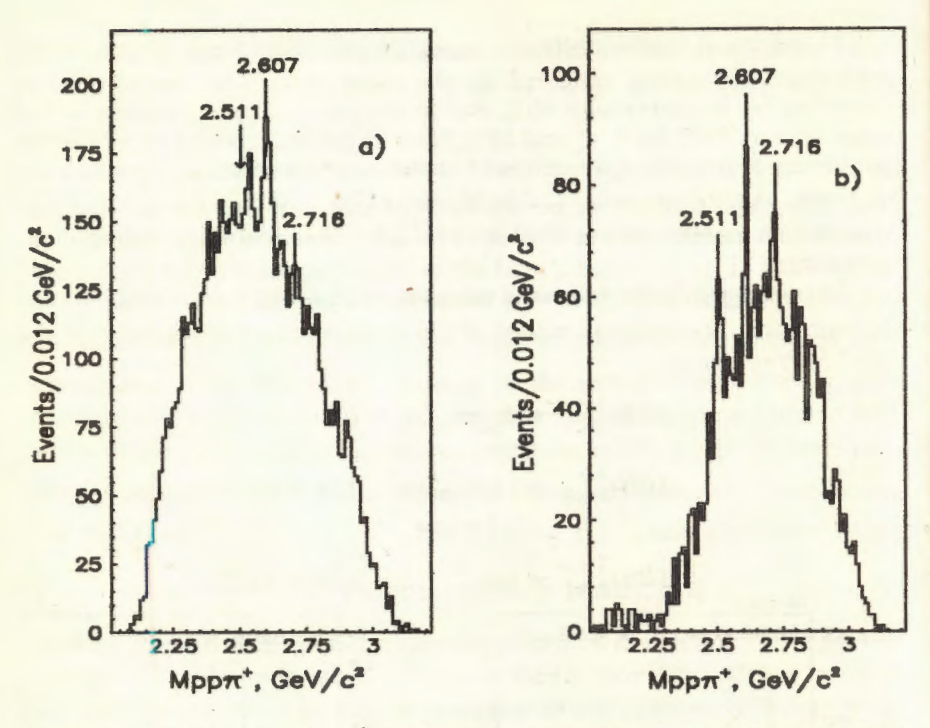


Fig. 4. a) — The distribution of  $pp\pi^+$  effective masses under the condition that at least one of the  $p\pi^+$ -combinations belongs to  $\Delta_{33}$ -isobar region (1.130  $\leq M_{p\pi}+ \leq$  1.296 GeV/c<sup>2</sup>). b) — The distribution of  $pp\pi^+$  effective masses under the condition that none of  $p\pi^+$ -combinations belongs to  $\Delta_{33}$ -isobar region ( $M_{p\pi}+ > 1.296$  or  $M_{p\pi}+ < 1.130$  GeV/c<sup>2</sup>)

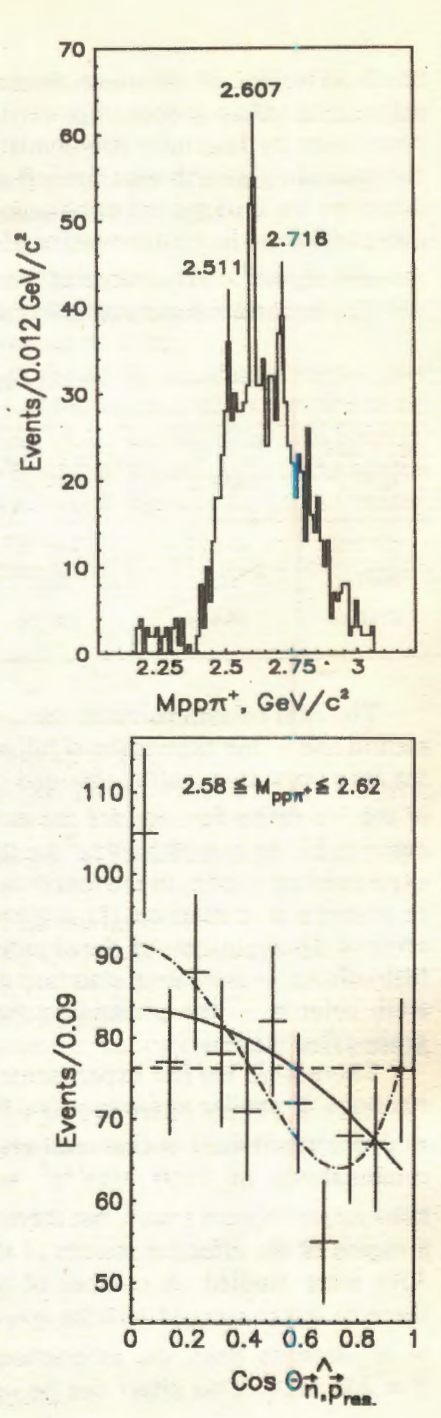
Figures 4 and 5 show the distributions of effective masses of  $pp\pi^+$ -combinations from reaction (5) for the events under some conditions for two — particle masses. The distribution of fig.4a was obtained by constructing  $pp\pi^+$  effective masses under the condition that at least one of the  $p\pi^+$ -combinations belongs to  $\Delta_{33}$ -isobar region (1.130  $\leq M_{p\pi}^+ \leq 1.296 \text{ GeV/c}^2$ ). The distribution of fig.4b was obtained by constructing  $pp\pi^+$  effective masses under the condition that none of  $p\pi^+$ -combinations belongs to  $\Delta_{33}^-$  isobar region ( $M_{p\pi}^+ > 1.296 \text{ or } M_{p\pi}^+ < 1.130 \text{ GeV/c}^2$ ). The distribution of fig.5 was obtained by constructing  $pp\pi^+$  effective masses under the condition that none of  $p\pi^+$ -combinations belongs to  $\Delta_{33}^-$  isobar region and under the additional condition that the effective masses of pp-combinations belong to the region of pp-resonance with a mass around 2.090 GeV/c<sup>2</sup>

Fig. 5. The distribution obtained by constructing  $pp\pi^+$  effective masses under the condition that none of  $p\pi^+$ -combinations belongs to  $\Delta_{33}$ -isobar region and under the additional condition that the effective masses of pp-combinations belong to the region of pp-resonance with a mass around 2.090 GeV/ $c^2$  (2.00  $\leq M_{pp} \leq$  2.20 GeV/ $c^2$ )

 $(2.00 \le M_{pp} \le 2.20 \text{ GeV/c}^2)$ . This distributions enable to research in more detail the discussion effects and to produce the quantitative marks of the probabilities of the different modes of decays.

To determine the spin of the  $2607 \text{ MeV/c}^2$  resonance, there was constructed and analysed the distribution of the angle between the normal of the resonance decay plane and the direction of resonance motion in general c.m.s. Such distributions are known-to be described in strong decays by a sum of Legendre polynomials of an even power with the maximum power of 2J, where J— the resonance spin, [3] (the angle is calculated in the resonance rest system). The distribution of  $\cos \Theta_{n}$ ,  $\frac{1}{p_{res}}$ , is shown in fig.6. There the dotted

Fig. 6. The distribution of  $\cos\Theta_{\vec{R},\vec{P}_{\text{pres.}}}$ —angle between the normal of decay plane of  $pp\pi^+$ -resonance with a mass 2607 MeV/ $c^2$  and the direction of its flight in general c.m.s.  $np \rightarrow pp\pi^+\pi^-\pi^-$ . All values are taken in resonance rest system. The dotted line—isotopic distribution, the solid line—the description by Legendre polynomials of up to second power inclusive, the dot-and-dash line—the description by Legendre polynomials of up to fourth power inclusive



line is an isotopic distribution, the solid line — the description by Legendre polynomials of up to second power inclusive, the dot-and-dash line — the description by Legendre polynomials of up to fourth power inclusive. The corresponding distribution for left and right sides is essentially isotopic, therefore the background subtraction was not carried out. The corresponding confidence levels are equal to 4%, 12% and 55%. Hence one may infer the spin of  $pp\pi^+$  — resonance at the mass  $2607 \text{ MeV/c}^2$  as  $J \ge 2$ .

The final data about the observed resonances are given in the Table.

Table

$M_e \pm \Delta M_e$ , MeV/c <sup>2</sup>	$\Gamma_e \pm \Delta \Gamma_e$ , MeV/c <sup>2</sup>	$\Gamma_R \pm \Delta \Gamma_R$ , MeV/c <sup>2</sup>	$\sigma \pm \Delta \sigma$ , $\mu b$	. S.D.	P
2511±5	46±21	24±21	8.4±3,0	4.0	5.0 · 10-4
2607±2	27±7	7±7	10.3±2,4	6.8	2.0 · 10-9
2716±4	36±16	22±16	4.9±2,2	- 3.4	1.4.10-2

The first column contains the central value of the resonance mass; the second one — the experimental full width of the resonance; the third one — the true resonance width, obtained by quadratic subtraction of the widths of the resolution function for the masses of  $pp\pi^+$ -combinations (these are equal to 23, 26 and 29 MeV/c² for the corresponding resonances) from the experimental widths. In the fourth column the cross-section of the resonance production in reaction (1) is given along with the errors, including the error of determination of the channel (1) cross-section (see [[1]); in the fifth column — number of standard deviations above the background, in the sixth column — the probability that observed enhancements are background fluctuations.

There were too few experimental data concerning searches and investigations of similar resonances in the previously published reports. The evidence about weak enchancements in the effective mass spectra of  $pp\pi^+$ -combinations at 2160 MeV/c² were obtained in [4,5]. In [6] no enhancements were found, but there either bound states of  $nn\pi^-$ -system or a region of the effective masses of the same system near the threshold of  $NN\pi$  were studied. A number of papers (see, e.g., [7] and references therein) was concerned with the investigations of the resonances production of  $\pi^+$ -mesons from the interactions of protons with various nuclei at  $T \approx 350$  MeV. This effect can be interpreted from the point of view of a

production and a following decay of resonances with isotopic spin I=2 proton-nuclei interactions, but there exist not less convincing alternative explanations.

One can note that all the above effects are observed in the mass regions placed considerably lower than that studied in our experiment.

Theoretical predictions about resonances with isotopic spin I=2 are made in the models using quite different approaches. There are predictions base on quark models [8], Skyrme model [9], the general quantum-mechanical approach in a model of semiopen resonator [10].

The very diversity of approaches with the whole spectrum of predictions signifies that the problem of the nature of the studied effect remains to be still open and requires considerably more experimental data to explain it. On the other hand it is very hard to overrate the significance of resonance effects in multihadronic (multiquark) systems, especially for the investigations of the relativistic nuclei interactions.

We are grateful to Dr.V.L.Lyuboshitz and Dr.V.I.Ilyushenko for helping us in our work.

## References

- 1. Besliu C. et al. Yad. Fiz., 1986, No.43, p.888.
- Troyan Yu.A. Fiz. Elem. Chast. At. Yadra, 1993, 24, p.683 (Phys. Part. Nucl., 1993, 24(3), p.294).
- Baldin A.M. et al. «Kinematics of Nuclear Reactions», M.: «Atomizdat», 1968.
- 4. Ermakhov K.N. et al. LRPI, 1158, Leningrad, 1986.
- 5. Combes-Comets M.P. et al. PRC, 1991, v.43, No.3, p.973.
- 6. Parker B. et al. PRL, 1989, v.63, No.15, p.1570.
- 7. Julien J. et al. Z. Phys., 1994, A 347, p.181.
- Mulders P.J., Aerts A.T., De Swart J.J. PRD, 1980, v.21, No.9, p.2653.
- 9. Nikolaev V.A., Tkachev O.G. Few Body Syst., 1991, 10, p.171.
- Gareev F.A., Ratis Yu.L., Strokovsky E.A. JINR, E2-93-426, Dubna, 1993.